A tunnel speleothem based stable-isotope record of Atlantic Multi-Decadal Oscillation forcing of precipitation in the Midlands, United Kingdom

A Thesis
SUBMITTED TO THE FACULTY OF THE
UNIVERSITY OF MINNESOTA
BY

Carolyn A. Shull

IN PARTIAL FULFILLMENT OF THE REQUIREMENTS
FOR THE DEGREE OF
WATER RESOURCES SCIENCE
MASTER OF SCIENCE

Dr. Howard Mooers, PhD

August 2019

Acknowledgments

Dr. Howard Mooers, Adviser

Committee members Dr. John Pastor and Dr. Byron Steinman. Mia O'Brien and Lydia at UMD Writer's Workshop for countless hours of proof reading and corrections. Dr. Laure Charleux for her GIS and Python tutelage. Dr. Salli Dymond and Dr. John Swenson for their introduction to isotopes. Dr. Latisha Brengman for assistance on the proposal and the use of microscopes. Dr. Ted Ozersky for assistance with coding in R. Dr. Phillip Larson for setting up Strater and chiming in. Dr. Tsutomu Shimotori at the UMD Research Instrument Laboratory. Aaron Lingwall, Robert Brown and Julia Halbur at Large Lakes Observatory for running analyses. Fellow grad students for reviewing writing and many discussions. Isocamp at the University of Utah. The Woodland Trust for their Nature's Calendar data. Anthony Sames and Liz Ross for the collection and recording of all water samples.

Correspondence concerning this article should be addressed to Carolyn Shull,

Contact: linnx069@d.umn.edu

Abstract

Cave speleothems are an established source of preserved data used in paleo-environmental reconstruction, as climate and land use information can be recorded in the carbon and oxygen isotopes. Speleothems in the tunnels of the canals in West Midlands, UK were investigated as another potential record as they appear to experience a rapid growth rate, a requirement to detect short-term climate events and low-amplitude climate signals. Formation in artificial structures restrict the potential record to the past 150 years, while other speleothem-based proxies span millennial time scales. Upon analysis, speleothem oxygen isotopes reflect the Atlantic Multi-Decadal Oscillation (AMO), and carbon and oxygen isotopes are correlated to land use changes. The results indicate speleothems from canal tunnels in central England potentially provide a record of land use changes and precipitation source water related to the AMO. Tunnel speleothem isotope data have the potential to serve as valuable datasets in climate teleconnection and modeling studies.

Table of Contents

List of Tables

List of Figures

Introduction

The Birmingham Canal Navigations (BCN) and the Staffordshire and Worcestershire Canal (SWC), built between 1772 and 1858, are systems of canals connecting the industrial areas of the Black County in the West Midlands, United Kingdom, and are part of the larger English canal system. Several tunnels were constructed along BCN and SWC networks including the Tardebigge, Shortwood, Wast Hills, Netherton, and Dudley tunnels. Water infiltrating through the country rock and into the tunnels has resulted in the formation of well-developed speleothems in the form of stalactites, soda straws, and flowstone. Some of these deposits have calcite accumulations of over 100 mm, suggesting accumulation rates on the order of 1 mm/year. The tunnels range from 530-2900 meters in length, which creates a stable, cave-like environment for speleothem growth with restricted airflow, constantly high humidity, and little annual temperature variation.

Stable isotopic analysis of oxygen and carbon of calcite in speleothems from caves are commonly used in paleoenvironmental studies to provide long-term records of variations in short-term climate (temperature and precipitation) and land use (farmland, industrial and residential) changes (Akers et al., 2016; Fairchild et al., 2006; Jex et al., 2010; Mattey et al., 2008). However, most cave speleothems have calcite accumulation rates of less than 1 mm/yr and so cannot resolve annual or even decadal oscillations in climate. Calcite accumulation rates of 1mm/yr, as in the tunnel speleothems, are unusual and have the potential to provide a high-resolution record of climate anomalies and/or environmental change. For recent speleothems such as these, isotope records are supported

by instrument climate data, historic land-use changes, and phenology records (Mattey, et al., 2008; Proctor et al., 2000).

Speleothems were collected from canal tunnels in the West Midlands, subsampled, and submitted for stable isotope analysis of calcite. The time series of speleothem oxygen and carbon isotopes are compared with climate records, including regional instrument station temperature and precipitation data, records of North Atlantic weather phenomena of the Northern Annular Mode (NAM) and North Atlantic Oscillation (NAO), the climate index of the Atlantic Multidecadal Oscillation (AMO), and historical air quality and land use changes. To evaluate local hydrology, rainwater from a surface sampling site and drip water from the Netherton Tunnel at one of the speleothem sampling sites was collected over a 13-month period and submitted for hydrogen (^{2}H, or deuterium) and oxygen (^{18}O) isotope analysis. Differences between the annual variation of precipitation and drip water isotopes are used to evaluate groundwater residence time and hydrologic pathways. The UK has a maritime climate influenced by numerous regional maritime and continental air masses (Mayes & Wheeler, 2013).

Instrument records from the United Kingdom indicate accelerated warming from 1960-1990 with temperatures increasing at a rate of 0.27 degree Celsius per decade (Kendon et al., 2017). This warming trend since the mid-1970s has affected the length of seasons, and is expressed in regional phenological data (Cotton, 2003; Kauserud et al., 2012; Sparks & Crick, 2015; Thackeray et al., 2010). Over a 30-year period, spring has advanced by 6 days across Europe while autumn arrives 4.8 days later (Mentzel & Fabien, 1999).

Results of this investigation suggest that oxygen isotopes provide a time series of changes in predominant oceanic sources of precipitation on the scale of the AMO. Furthermore, correlation of $\delta^{18}O$ with land use indicates a seasonal variation in infiltration biased toward the cold season. Carbon isotopes are difficult to interpret and suggest multiple phases of exchange with ancient carbon during infiltration through the vadose zone prior to calcite precipitation.

Background

Speleothems

Speleothems serve as environmental archives as they contain stable isotopes of oxygen ($\delta^{18}O$) and carbon ($\delta^{13}C$), the proportion of which is responsive to environmental variables, such as temperature, rainfall, air quality, and local vegetation cover and type (Fairchild et al., 2006). Speleothems are widely used in paleoclimate studies because they provide records of climate and the physical environment in stratified layers that potentially provide chronology. In addition, organic compounds are often incorporated in the calcite of speleothems and can be used as environmental proxies (Blythe et al., 2016). There are currently no independent, high-resolution climate proxies spanning the past 150 years in the central England region; instead, existing speleothem-based proxies in the UK span millennial time scales (Kashiwaya et al., 1991; Baker et al., 1995). Because of their rapid growth rates, tunnel speleothems might provide a high-resolution record of climate and land use since tunnel completion in the mid-1800s.

Because of the maritime setting, the isotope characteristics of meteoric precipitation reflect source water from the north Atlantic region surrounding the UK.

Additionally, periodic weather phenomena such as the NAO, NAM and cyclic changes in climate-driven AMO affect the source of precipitation and therefore the isotope composition.

Speleothem formation in underground caverns depends on the percolation of water through overlying rock (Figure 1). Meteoric water infiltrates and equilibrates with soil CO_2 with a P_{CO2} of about 10^{-2} (Hendy, 1971). With further infiltration, the water dissolves carbonates in the rock and becomes saturated with calcite, $Ca(HCO_3)_2$.

$CO_{2\,(g)} \leftrightarrow CO_{2\,(aq)}$	Diffusion of CO_2 into water	[1]
$CO_{2(aq)} + H_2O_{(l)} \leftrightarrow H_2CO_3$	Formation of carbonic acid	[2]
$H_2CO_3 \leftrightarrow H^+ + HCO_3^-$	Formation of bicarbonate	[3]
$CaCO_{3(s)} + H_2O_{(l)} + CO_{2(aq)} \rightarrow Ca(HCO_3)_{2(aq)}$	Dissolution of bedrock	[4]

The saturated solution continues to percolate through fractures and pores in the rock. Speleothems grow through the precipitation of calcium carbonate ($CaCO_3$) as the carbonate solution drips into the cave. Evaporation or degassing of CO_2 increases Ca^{2+} concentration until $CaCO_3$ is no longer soluble. Evaporation occurs near cave entrances, where there is exchange of saturated and unsaturated air. Degassing is the prominent mechanism in the depths of caves where relative humidity remains near 100%. Evaporation and degassing drive the reaction to deposit calcium carbonate:

$HCO_3^- \leftrightarrow H^+ + CO_3^{2-}$	Formation of carbonate	[5]
$Ca(HCO_3)_{2(aq)} \rightarrow CaCO_{3(s)} + H_2O_{(l)} + CO_{2\,(aq)}$	Formation of calcium carbonate	[6]

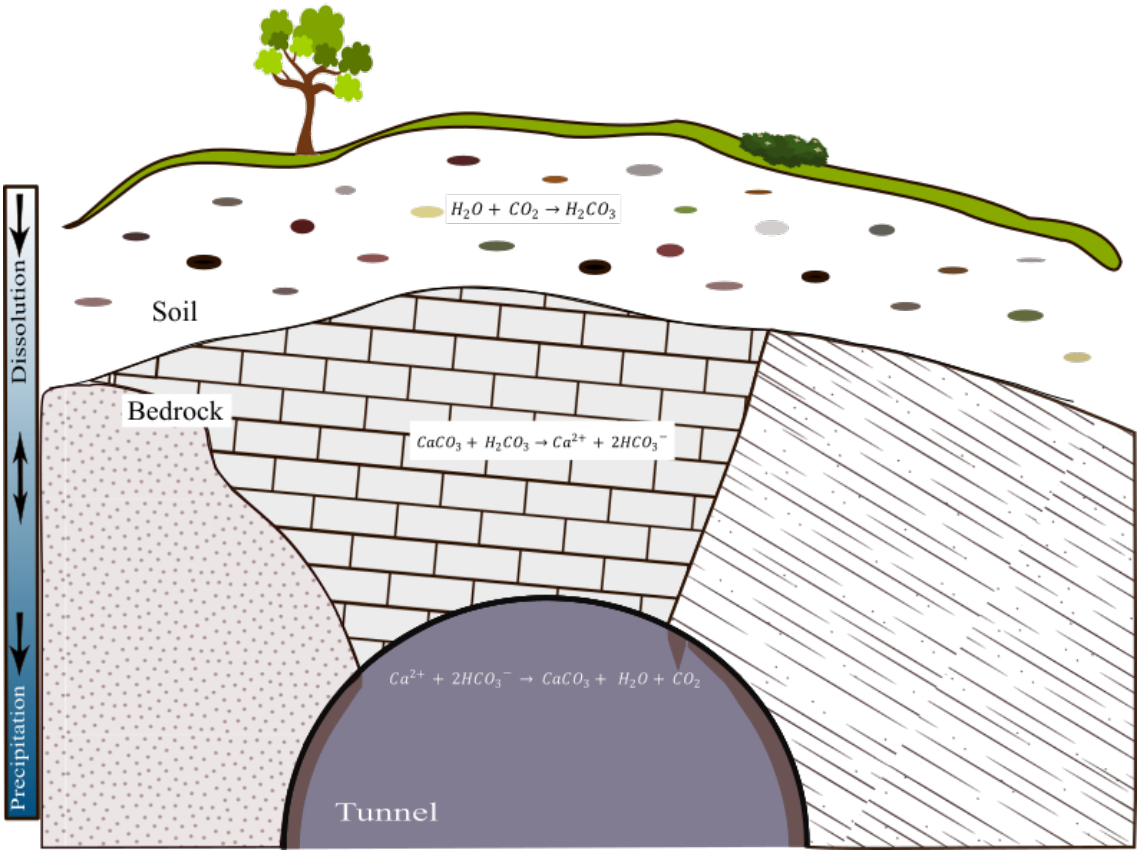

Figure 1. Tunnel Schematic

The trace element strontium (Sr) can be incorporated in calcite as a substitute for Ca when Ca availability is restricted (Fairchild et al., 2000). Higher Sr/Ca ratios occur at lower drip rates, increasing Sr concentration during dry conditions with more rapid calcite precipitation (Fairchild et al., 2000; Johnson et al., 2006; Huang, et al, 2001).

Stable Isotopes in Speleothems

The relative abundance of the heavy isotope in a sample, compared to a standard, is represented by the delta notation, $\delta^{18}O_x$ or $\delta^{13}C_x$, in per mil (‰), and is calculated as:

$$\delta^{18}O = \{[(^{18}O/^{16}O)_{sample}/(^{18}O/^{16}O)_{Standard}]-1\}*1000 \quad [7]$$

$$\delta^{13}C = \{[(^{13}C/^{12}C)_{sample}/(^{13}C/^{12}C)_{Standard}]-1\}*1000 \quad [8]$$

There are two international standards for measuring ratios of $\delta^{18}O$; Vienna Peedee Belemnite (VPDP) or Vienna Standard Mean Ocean Water (VSMO). It is convention, however, to report $^{18}O/^{16}O$ in VPDP when working with carbonates. VPDP is also the standard for $\delta^{13}C$, which is measured concurrently with $\delta^{18}O$ during analysis via isotope-ratio mass spectrometry (IRMS). The IRMS precision of both $\delta^{18}O$ and $\delta^{13}C$ analyses is typically ±0.1‰.

When speleothems form in oxygen isotope equilibrium with drip water, the temperature at the time of precipitation is incorporated in the isotopic record. The paleotemperature equation (Epstein et al., 1953) provides the formation temperature:

$$T(°C) = 16.5 - 4.3(\delta^{18}O_{calcite} - \delta^{18}O_{H2O}) + 0.14(\delta^{18}O_{calcite} - \delta^{18}O_{H2O})^2 \quad [9]$$

In general, equilibrium conditions are most likely met at sites far from entrances or openings, with a relative humidity of approximately 100%, stagnant air resulting in high PCO_2, and constant seasonal temperatures that mimic the overlying surface mean annual temperature (Schwarcz, 2007). In these conditions, equilibrium deposition should provide a record of surface temperatures (Schwarcz, 2007).

In-cave evaporation, temperature, and drip rate influence the formation of speleothems and their role in recording climate (Day & Henderson, 2011). Kim and O'Neil (1997) determined the oxygen isotope equilibrium fractionation factor for the precipitation of synthetic calcite:

$$1000\ln\alpha(\text{calcite-water}) = 18.03(1000/T) - 32.42, \quad [10]$$

where α is the fractionation factor expressed in convention with the delta value per mil, and T is the temperature in degrees Kelvin (Clark & Fritz, 1997; Kim & O'Neil 1997).

The temperature-dependent fractionation of oxygen in isotopic equilibrium represents the proportion of elevated concentrations of heavier isotopes in calcite, which form relatively stronger covalent bonds. Greater dissociation energy is required to release the heavier oxygen isotope. The ^{18}O is, therefore, preferentially incorporated in the solid state of calcite. To resolve residual uncertainty regarding speleothem formation in equilibrium or evaporative conditions, equation 10 for oxygen isotope equilibrium fractionation between water and calcite can be applied at any given temperature (Kim & O'Neil, 1997).

Low temperature, fast dripping, and high humidity environments experience the most growth, providing favorable controls for paleoclimate studies (Day and Henderson, 2011). At low temperatures and high drip rates, temperature has a greater impact on growth than drip rate (Day and Henderson, 2011; Genty et al., 2001). With higher degassing rates, speleothems become enriched in $\delta^{18}O$ (Hendy, 1971). Growth rate is strongly correlated to the mean annual temperature of the overlying surface and drip water calcium ion concentrations, both sensitive to soil CO_2 levels (Genty et al., 2001). Seasonal variations in growth rates are related to site hydrology and generally demonstrate similarities from year to year (Genty et al., 2001).

Two controls impact the $\delta^{18}O$ of calcite in speleothems. First, mean air temperature (MAT) at the terrain surface is positively correlated to the $\delta^{18}O$ of precipitation at mid- to high-latitudes (Dansgaard, 1964; Rozanski et al., 1993) and meteoric water is the conduit.

There are 10,000 times as many oxygen atoms in water than in any of the carbonate phases (Dreybrodt, 2008). Therefore, the oxygen isotopes from the water dominate isotopic equilibrium (Dreybrodt, 2008). The second control is the cave, or in this case tunnel, temperature which is negatively correlated to calcite $\delta^{18}O$ (Duplesy et al., 1970; Schwartz, 1986; Gascoyne, 1992).

Fluctuations in the $\delta^{13}C$ signal represent variations in carbon sources and mixing processes during dissolved inorganic carbon (DIC) formation, and are not significantly temperature dependent (Schwartz, 2007). Carbon in speleothem calcite under ideal conditions has two sources: atmospheric and soil CO_2, and DIC from dissolution of carbonate along the path of infiltration (Figure Tunnel Drawing). However, there are many factors that influence the isotopic ratios of ^{12}C, ^{13}C and potentially ^{14}C.

Atmospheric concentrations of CO_2 at present are about 400 ppm ($10^{-3.4}$) with a $\delta^{13}C$ of -7 to -8 ‰ (Team, 2005; Clark & Fritz, 1997) (Figure 2). Soil atmosphere is enriched in CO_2 from microbial respiration and has concentrations of about 10,000 ppm or 1% (10^{-2}). The contribution of atmospheric P_{CO2} to the isotopic composition of DIC is negligible when compared to soil P_{CO2} and thus meteoric waters equilibrate with soil P_{CO2} as they infiltrate the subsurface (Clark & Fritz, 1997). The soil CO_2 isotopic ratio of $^{13}C/^{12}C$ ($\delta^{13}C$) is highly dependent on the source of carbon involved in microbial metabolism.

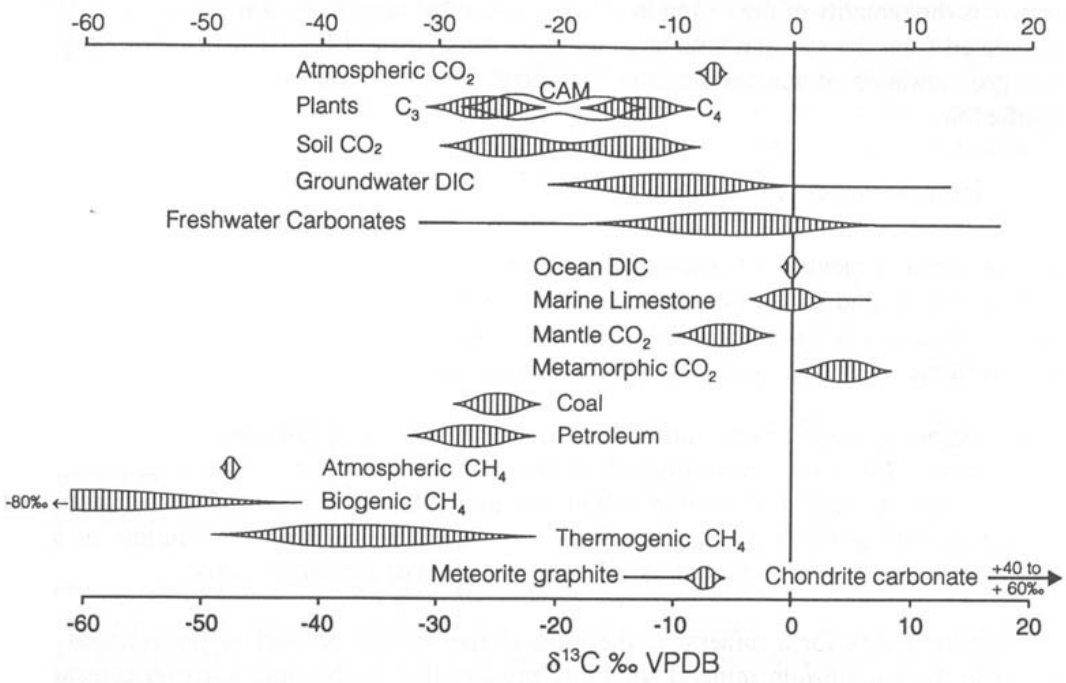

Fig. 5-1 Ranges for $\delta^{13}C$ values in selected natural compounds. Especially noteworthy is the spread in ^{13}C seen in different plant groups and the resulting soil CO_2.

Clark & Fritz, 1997

Figure 2. Carbon Isotope Ranges

Plants have two different photosynthetic pathways, C_3 and C_4. The C_3 photosynthetic pathway results in a $\delta^{13}C$ range of -24 to -30 ‰, whereas the C_4 photosynthetic pathway results in $\delta^{13}C$ values of -10 to -16 ‰.

The UK consists of C_3 landscapes. C_3 vegetation includes most crops and plants native to temperate regions at high latitude, as well as tropical forests. These processes result in an overall depletion in C_3 plant ^{13}C of approximately 22‰ and the $\delta^{13}C$ of the CO_2 in C_3 soils is typically -23‰ (Clark & Fritz, 1997).

The $\delta^{13}C$ of dissolved carbonate is generally very close to VPDB ($\delta^{13}C = 0.0$) reflecting marine limestone. Therefore, the $\delta^{13}C$ value of DIC in infiltrating waters formed

by soil CO_2 in a C_3 environment dissolving marine limestone would typically range from -12 to -15 ‰. However, there are many factors that influence $\delta^{13}C$ in DIC.

1. Carbonate in the vadose zone may be secondary carbonate and not primary marine carbonate.
2. Burning of fossil fuels, particularly coal, pollutes the atmosphere with ancient carbon with a $\delta^{13}C$ value of -28‰ (Team, 2005). In addition, detrital soot from coal burning can affect soil CO_2.
3. Microbial decomposition of ancient carbon such as coal or other detrital carbon deep within the vadose.
4. Multiple generations of precipitation and dissolution in the vadose zone.

During an investigation of speleothem samples from a British cave system, as well as a review of analyses of speleothem samples from Great Britain, Baker et al. (1997), noted elevated $\delta^{13}C$ values over the expected range (-12 to -6 ‰) for a C_3 landscape. Additionally, they observed 17% variability, approximately one standard deviation, in the $\delta^{13}C$ signal. These results have three potential causes. First, evaporation or degassing during the growth of cave formations causes isotopic fractionation. Secondly, the degassing of groundwater before it reaches the cave maintains calcium levels while CO_2 is released. Lastly, short residence time of water in the soil does not allow for equilibrium between soil H_2O and soil CO_2 to be achieved. Care is therefore necessary when interpreting the $\delta^{13}C$ values of speleothems with respect to paleovegetation (Baker et al., 1997).

The Suess Effect refers to the decrease in ^{13}C and ^{14}C resulting from the combustion of fossil fuels, and represents the dilution of isotopic carbon by anthropogenic activity.

Fossil fuels are depleted in ^{13}C and as coal is largely composed of C3 vegetation (Farquhar et al.,1989) and is extremely old.

Interpreting the isotope signature of speleothems is challenging, as abundant controls on both carbon and oxygen isotopes are present during the evolution from source water to speleothem (Lachinet, 2006). For example, isotopic composition of cave drip water is likely affected by mixing along different paths through the bedrock (Long & Putnam, 2004). Mixing dampens the $\delta^{18}O$ signal, and therefore the $\delta^{18}O$ of the calcite integrates or averages the composition of precipitation over the residence time in the vadose zone (Lachinet, 2006).

In the role of archiving climate trends, translating speleothem records is often difficult during less pronounced climate shifts and shorter periods. Employing more than one proxy and investigating the mechanism of formation improves the interpretation process as variations in signals caused by long-term climate, mid-range seasonal and short-term weather effects, as well as additional environmental factors, are all encoded in speleothems. Fairchild et al. (2006) cites five major factors influencing speleothem geochemistry. The atmosphere, vegetation/soil, karstic aquifer, and initial deposition, along with modification of speleothem layers, all offer contributions to speleothem growth that mask the direct impact of climate. Growth from different seasons and their proportional changes over time act as indicators of seasonal variation. Longer time period signal fluctuations likely describe synoptic processes that trigger specific isotope signals, and thus trends in the frequency of weather types. Carbon and trace element signals derived

from the overlying soil and ecosystem can display variations over time that mirror the history of land use and other changes (Fairchild et al., 2006).

Stable Isotopes of Water: The Evolution of Oxygen and Hydrogen Isotopes from Source Water to Precipitation.

The stable isotopes, ^{18}O and deuterium, or ^{2}H, can be used to characterize air masses and identify various source waters and thus the origin (Gat, 1971). Numerous studies have investigated the effect of evaporative processes from surface waters on oxygen and hydrogen isotopes (e.g. Gat, 1971; Craig & Gordon, 1965; Gonfiantini, 1986). A thin saturated boundary layer maintains isotopic equilibrium with the water surface below. In a transition zone above the boundary layer, fractionation during bi-directional molecular diffusion of water vapor determines isotopic enrichment or depletion in the liquid and atmosphere, respectively (Figure 3) (Clark & Fritz, 1997). The fractionation between the water body and the atmosphere is, therefore, the sum of the equilibrium isotope fractionation in the boundary layer, and in the transition zone, the kinetic fractionation from diffusion into the air column as well as that from the return of atmospheric moisture (Gat, 1996; Clark & Fritz, 1997). Evaporation results in the water becoming enriched with the heavier isotopes of both oxygen and hydrogen while the vapor becomes depleted (Gat, 1971). Because of its greater mass, the kinetic fractionation of ^{18}O exceeds that of ^{2}H, while equilibrium fractionation of ^{2}H remains much greater than that of ^{18}O. The relationship of $\delta^{18}O$ to $\delta^{2}H$ is thus variable, and water bodies influenced by evaporation are identified by lower slopes than the slope of ~8 of the Global Meteoric Water Line (Clark & Fritz, 1997, pg 43). Various humidity levels cause variation in the ^{2}H values of precipitation; the

difference from seawater is termed deuterium excess. Fractionation depends on surface temperature, vapor pressures of the various isotopologues, wind shear and associated water turbulence, and, most of all, relative humidity. The isotopes in the vapor experience additional modification during the formation of an air mass as evaporated water vapor mixes with water vapor resulting from previous condensation and precipitation over the ocean (Craig & Gordon, 1965; Gat, 1996).

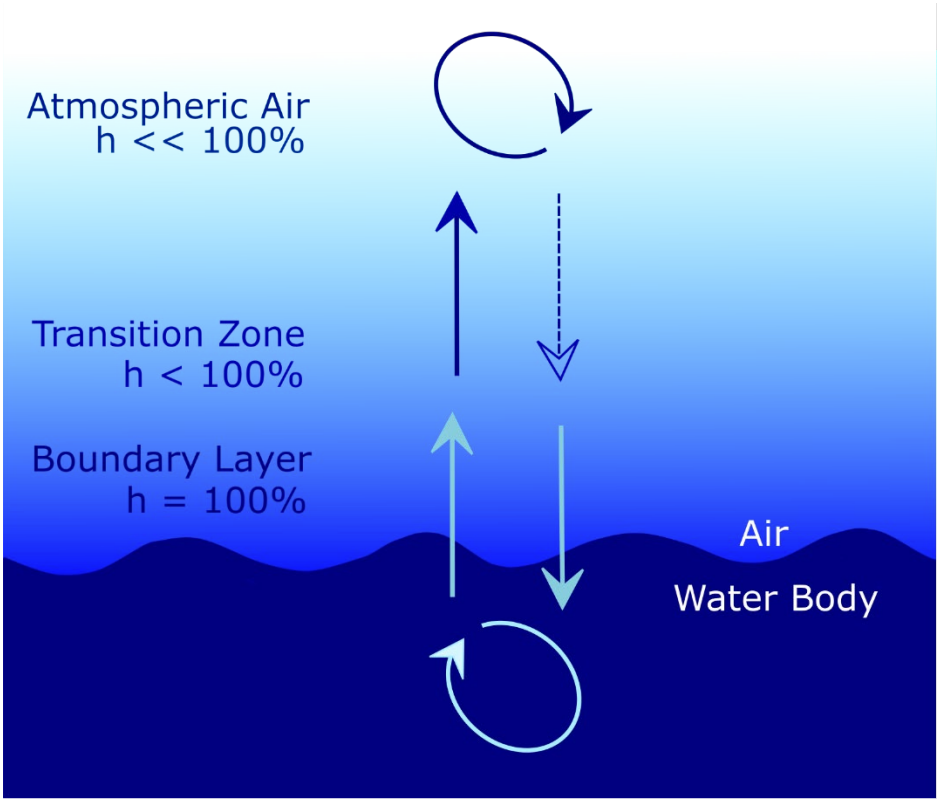

Figure 3. Non-equilibrium evaporation at the water-air interface. Relative humidity levels (h) within each layer are denoted.

The temperature of an air mass decreases as it migrates to higher latitudes, or experiences adiabatic cooling during orographic lifting over land masses, and vapor condenses as precipitation, or "rain out." Precipitation is an equilibrium process in the cloud (h = 100%) during which equilibrium fractionation occurs and preferentially

incorporates ^{18}O and ^{2}H in the condensate (Gat, 1971). The isotopic difference between phases is expressed in Figure 4 as the enrichment factor (ε). Isotopically enriched water molecules are removed from the air mass and the remaining vapor becomes depleted in the heavier isotopes. This process, Rayleigh distillation, continues as subsequent precipitation is further depleted compared to earlier precipitation from the same air mass (Gat, 1971; Clark & Fritz, 1997). Rain-out, therefore, creates progressive isotopic depletion of the heavy isotopes in precipitation. Temperature and Rayleigh distillation impact the $\delta^{18}O$ and $\delta^{2}H$ values of meteoric water (Dansgaard, 1964; Sharp, 2017). The distance from source water, greater in higher latitudes and over the interior of continental land masses, altitude and seasons contribute to the degree of Rayleigh distillation.

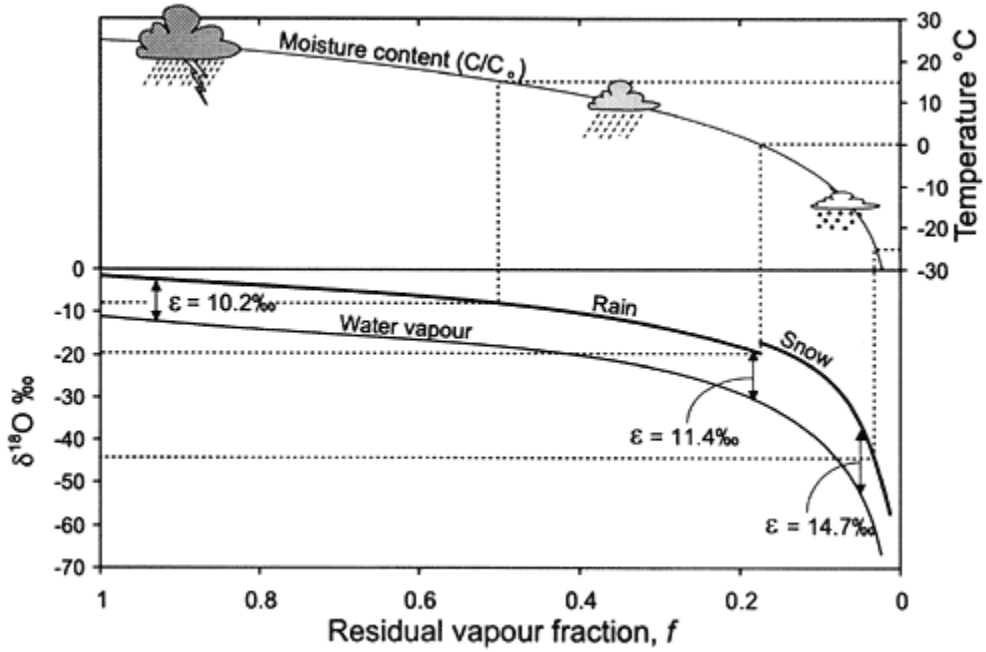

Figure 4. Isotopic evolution of Rayleigh distillation during rainout in a closed system. Clark & Fritz, 1997

Climate in the United Kingdom

The United Kingdom is situated in the high mid-latitudes, and experiences a maritime climate that is typically cool and cloudy, with infrequent temperature extremes. At least six major air masses influence the climate of the United Kingdom (Mayes & Wheeler, 2013) as depicted in Figure 5.

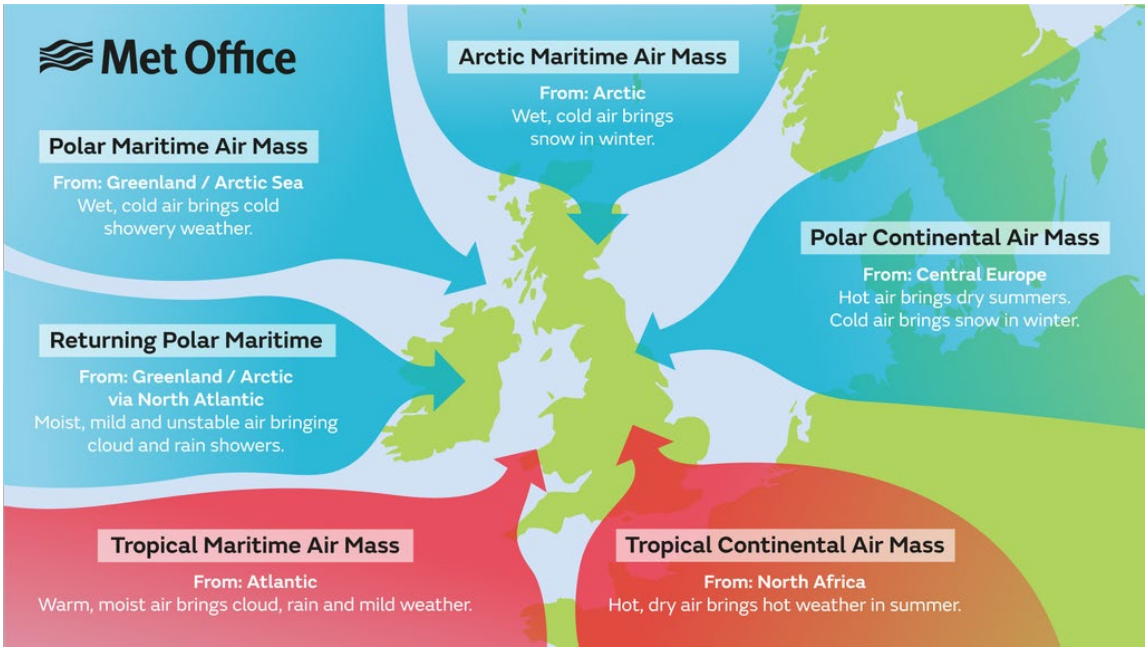

Figure 5. Air Masses

Climatic teleconnections in the UK are influenced by three major weather and climate cycles that vary the source of precipitation and therefore isotopic composition. The Arctic Oscillation (AO) (or Northern Annular Mode, NAM) and the North Atlantic Oscillation (NAO) are non-periodic, high frequency weather anomalies related to sea-level atmospheric pressure. The Atlantic Multi-Decadal Oscillation (AMO) is a climate cycle that affects sea-surface temperatures on a multi-decadal scale.

Artic Oscillation or Northern Annular Mode. The NAM is a weather index with no periodicity that describes sea level pressure (SLP) anomalies between the arctic and the

mid latitudes. A positive NAM index represents low surface pressure in the Arctic; in this mode, the jet stream remains consistent in strength and direction and Arctic air masses are generally restricted north of the Arctic Circle. Higher pressure at mid-latitude forces ocean storms northward, delivering wet weather to the United Kingdom and dry conditions to the Mediterranean. High pressure (a negative NAM index) in the Arctic leads to greater meridional flow of the sub-polar jet stream, causing a southern incursion of cold air into the mid latitudes. The United Kingdom, then, experiences much colder and drier conditions.

North Atlantic Oscillation. The NAO refers to non-periodic fluctuations in the difference of sea level pressure (SLP) between the Subpolar (Icelandic) Low-pressure system in the Arctic and the Subtropical (Azores) High-pressure system in the northern mid-Atlantic. With varying intensities, both pressure systems compete for control of winds and weather tracks over the Northern Atlantic. They also influence temperatures, storm activity and precipitation across the North Atlantic, North America, Europe, Western Asia and the Mediterranean.

A positive NAO index indicates a strengthening of both the Icelandic Low and the Azores High. This results in below normal pressures at high latitudes and above normal pressure over central North Atlantic and Western Europe. These conditions result in strong westerly winds that direct moisture over northern Europe resulting in mild temperatures during summer and winters, and frequent precipitation. A negative NAO index results in the opposite conditions: above normal pressure near the Arctic and below normal pressure at mid-latitude. These conditions cause harsher temperatures, hotter summers and colder

winters, drier conditions, and storms that track over the Mediterranean region to the south (Rodwell et al., 1999).

Atlantic Multidecadal Oscillation. The AMO is a cycle of recurring changes in sea surface temperatures (SST) in the North Atlantic Ocean (0-80N) that occurs over several decades, on the order of 20-40 years (National Oceanographic and Atmospheric Administration (NOAA)) to 60-80 years (Trenberth and Zhang, 2019) (Figure 6). The AMO index is persistent over multiple instrument and reconstructed SST datasets (Trenberth and Zhang, 2019). Trends in mean surface temperatures and rainfall in the northern hemisphere, especially associated with the summer climate across Europe, correspond to the AMO. Shifts from cold (negative AMO) to warm (positive AMO) phases are correlated to warming periods in the Northern Hemisphere (Zampieri, 2017).

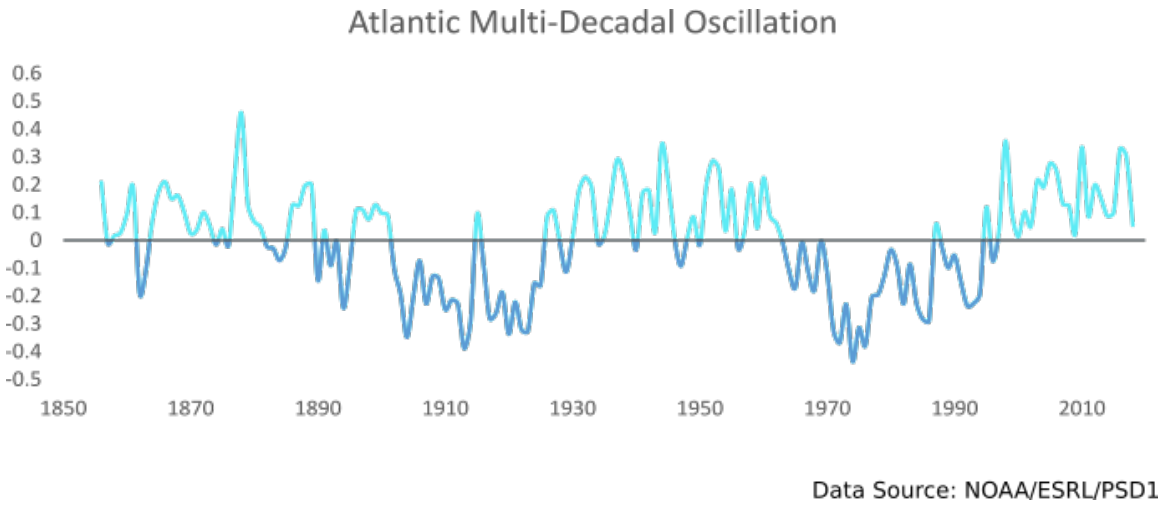

Figure 6. The Atlantic Multi-Decadal Oscillation

Air quality. Air quality in the Midlands, UK, has been reconstructed for the period 1890 to 2010 (Mooers et al., 2016). Coal burning over this period had a significant impact

on air quality resulting in high SO_2 and particulate (soot) concentrations. Soot from coal burning contributes ancient carbon to soils.

Temperature and Precipitation

Central England Temperature. The Central England Temperature (CET) record is the longest instrument station temperature record in existence, spanning from 1772 to the present. The dataset is compiled from the three stations (Figure 7): Stoneyhurst in Lancashire, Pershore in Worchestershire and Rothamsted in Hertfordshire (Met Office, 2018). This long-term temperature record has been corrected for data gaps, heat island effect, station closures, and short-term variability (Parker et. al, 1992).

Central England Precipitation. The HadUKP data set is the longest instrument record of precipitation in existence. Initial collection, the England and Wales Precipitation (EWP) record, was started in 1766 and continues to the present. The EWP consists of weighted precipitation totals from a network of stations spanning five regions in England and Wales. Multiple studies have updated and revised the record (Craddock, 1976; Manley, 1977; Wigley et al., 1984; Simpson & Jones, 2011).

Historical Station Data. The Met Office also maintains Historic Station Data, which include individual station records from Ross-On-Wye, Coventry, City Hospital, Edgebaston, Shawbury, Sutton Bonnington and Oxford (Figure CET and Individual Stations). The data include the monthly temperature minimum (Tmin), maximum (Tmax), and average (Tavg) and precipitation totals (Met Office, 2017).

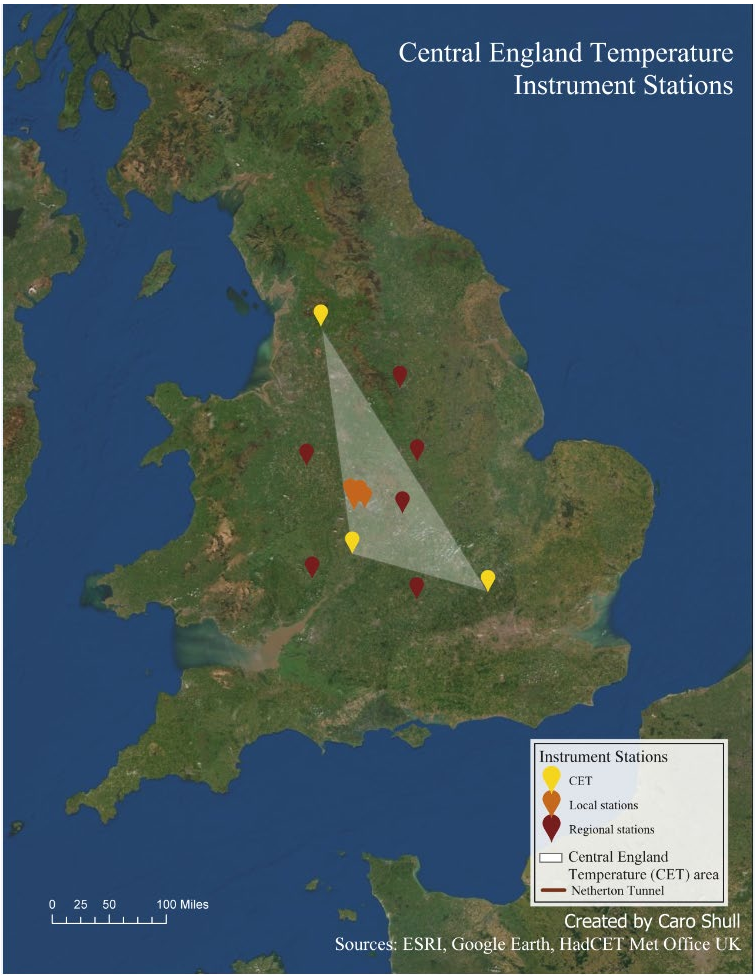

Figure 7. Location of stations for CET and Historic Station Data

Dating Speleothems

Chronology is critical for comparison of speleothem proxies with instrumental climate data and environmental parameters to recognize potential relationships. Radiometric dating can be used to determine annual layering (Tan et al, 2014; Baker 2008).

Uranium-series dating is the most common method of dating speleothems samples (Tan et al, 2014; Spotl & Boch, 2012). The uranium (U) levels in calcite

speleothems typically fall between 100 and 1000 parts per billion U (Schwartz, 2007). The parent isotope, ^{238}U, is water-soluble and precipitates with calcite. The daughter isotope, ^{230}Th is insoluble and adsorbs onto particles. When uranium is integrated in the calcite crystal, a zero $^{230}Th/^{238}U$ ratio exists before ^{238}U begins to decay.

The secular equilibrium along the growth axis determines the age of the calcite. Calcite speleothems tend to consist of large crystals that maintain their initial structure after deposition (Schwartz, 2007), preserving the record. U-series analysis is accomplished via thermal ionization mass spectrometry (TIMS). Higher U concentration, increased speleothem age, and a lack of detrital contamination from cave flooding all lower the uncertainties in the initial $^{230}Th/^{232}Th$ ratio and increase precision (Dorale et al., 2004). Instrument contamination and high levels of error, however, can result from detrital material and organics in carbonates (Blythe et al., 2017).

^{210}Pb dating techniques are commonly used on samples younger than 150 years. Since ground water and drip water in caves have high concentrations of ^{222}Rn, recent speleothem growth should contain excess ^{210}Pb in sufficient quantities for radiometric age determination (Baskaran and Iliffe, 1993). Multiple challenges accompany this method, such as variable lead concentrations and large sample size requirements (Baskaran, and Iliffe, 1993; Tan et al, 2014; Tanahara; Akira, et al., 1998).

Radiometric dating of ^{14}C often produces a timeline of speleothems. When speleothems form in hyperalkaline conditions, atmospheric characteristics are preserved as the carbon and oxygen atoms dissociate at a slower rate (Hartland et al., 2014). Speleothem

^{14}C content is impacted by atmospheric radiocarbon and the atmospheric bomb peak may be recorded. Therefore, analysis of young speleothems seeks to identify the increase in atmospheric carbon resulting from H-bomb testing that occurred between 1950 and 1963 (Hodge et al., 2011; Tan et al. 2014), versus radiometric dates (I. Fairchild, personal communication, March 2-3, 2019).

Annual laminas provide an age model for paleoclimate information in speleothems. Layers formed by fluctuations in annual cycles of organic matter can be identified with confocal laser microscopy (Tan et al, 2014; Baker et al, 2008; Baker et al, 1999). Laminae identified by variations in the texture and fabric of calcite deposits are visible with transmitted and reflected light microscopy (Tan et al, 2014; Baker et al, 2008).

Annual layering in speleothems can also be identified by annual cycles in the strontium-calcium (Sr/Ca) ratio. (Tan et al. 2014, Johnson et al., 2016). During dry periods, speleothem Sr/Ca and $\delta^{13}C$ are enriched by the relative unavailability of Ca in solution (Johnson et al., 2006). Enrichment can occur from a lower drip rate causing a higher rate of CO_2 degassing and calcite precipitation. Enrichment can also result when Ca precipitates in the bedrock or cave ceiling prior to reaching the speleothem. Both processes are associated with drier conditions (Johnson et al., 2006).

Study Area

The Birmingham Canal Navigations

The extensive canal system in England, which was established in the mid-1700s, but was replaced by the railway less than a century later. Currently the canal network is

maintained for recreation and tourism. The Birmingham Canal Navigations (BCN), in the West Midlands, England, is a network of canals that connects Birmingham to Wolverhampton and the Black Country and at specific junctions, the rest of the British canal system. The BCN was created on three primary levels connected by locks. Originally, vessels that travelled the canals were towed by oxen, men, or horses from an adjacent towpath. Although boats are now self-powered (diesel), the towpaths remain as trails.

Tunnels

The canals incorporate tunnels to avoid high-relief terrain. Three tunnels in the BCN were the focus of this investigation. The Shortwood Tunnel, is located seventeen kilometers south of Birmingham and is 560 meters long. The Shortwood tunnel lies in a region of mildly-deformed sandstone and mudstone, with speleothem formation associated with a fracture network near the southern entrance of the tunnel.

Between the Shortwood Tunnel and Birmingham is the Wast Hills tunnel, constructed in 1797, with a length of 2,493 m. The overlying bedrock consists of undeformed, homogeneous mudstone, and there are no significant geological structures in the vicinity, consequently no substantial speleothem growth occurs along the tunnel.

Eleven kilometers to the west of Birmingham, Netherton Tunnel, spans 2,768 m through Tansley Hill. The Netherton Tunnel was opened in 1858 and the overlying Etruria Formation.

The Etruria Formation underlies much of the Black Country of the West Midlands. Red beds comprised of calcareous red mudstones and sandstones overlie and are

interdigitated with the coal bearing grey beds of the Upper Carboniferous Coal Measures (Besley & Turner, 1983; Besley & Cleal, 1997; Geology of the West Midlands Branch Area, 2011) (Figures 8 and 9). The Etruria Formation overlying the Netherton Tunnel has undergone significant deformation and is characterized by networks of faults and fractures (Figures 8 and 9).

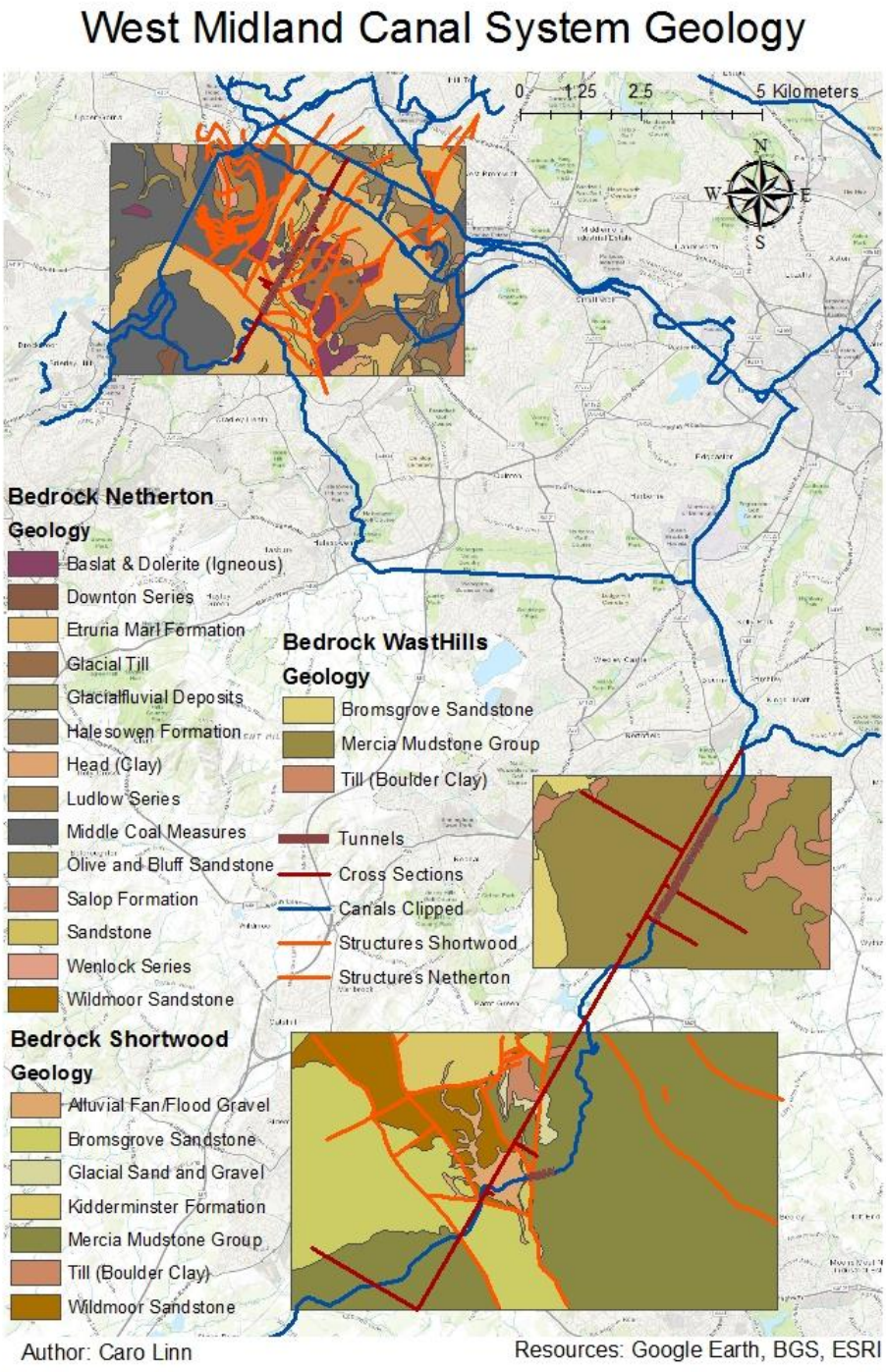

Figure 8. Tunnel Geology

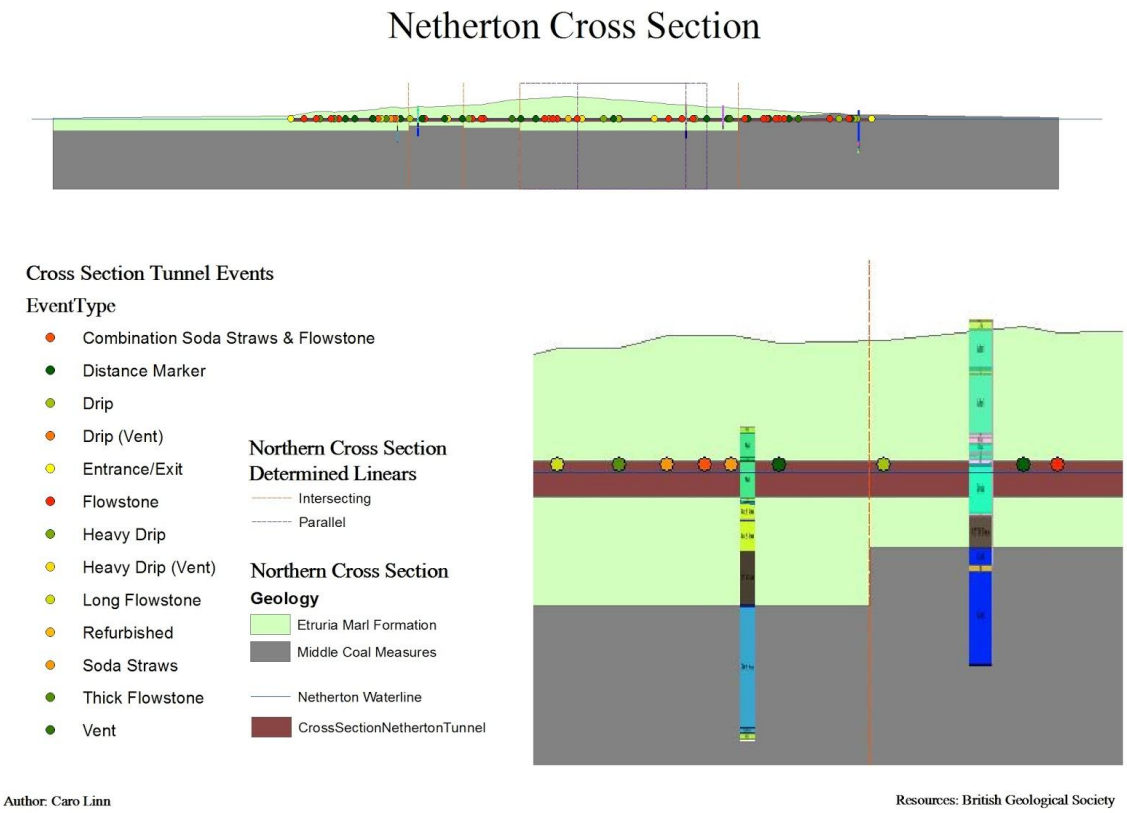

Figure 9. Netherton Tunnel Cross Section

Geology and Speleothem Formation

Groundwater seeping through carbonate bedrock above the tunnels has formed multiple types of speleothems on the tunnel brickwork. The drip water results in both sheet-like deposits, called flowstone (Figure 10, Figure 11 and Figure 12), as well as dripstone, which can be in the form of stalactites or soda straws (Figure 13) soda straws and Stalactites) on the tunnel ceilings and walls. Thin flowstone and soda straws are not suited to paleoclimate studies; layering tends to be inconsistent while soda straws experience dissolution and re-deposition of calcite (Self & Hill, 2003). The stalactites and areas of

thick flowstone in the canal tunnels, however, are extensively developed with thicknesses of 10 cm or more; given the age of the tunnels, deposition rates over 0.5 mm/year are indicated (Figure 13).

Figure 10. Thin Flowstone

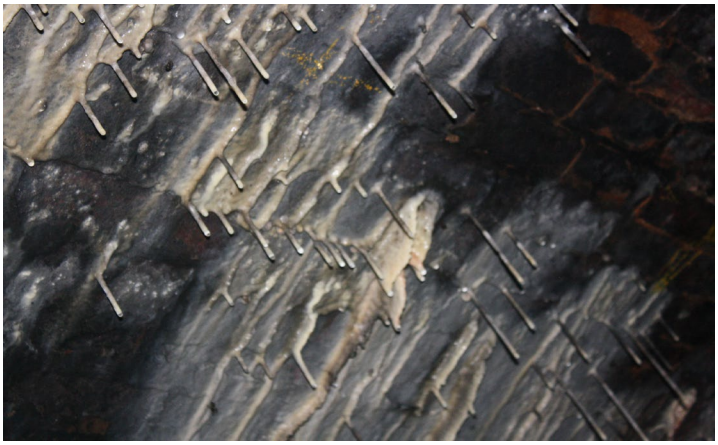

Figure 11. Soda Straws and stalactites

Figure 12.Thick Flowstone

Figure 13. Thick Flowstone Close-Up

Methods

Event Log and Mapping

A diesel-powered narrowboat served as a platform for tunnel investigation and sample collection. A record of tunnel features including speleothem formations, drip rates and other points of interest was created via a constant-speed, timed transit of the tunnel via narrowboat. The motor was run at idle to produce a constant, slow traverse of the length of the tunnel and total time of passage was applied to determine the motoring speed, which was subsequently used to calculate the location of each event based on the time it was recorded.

Speleothem Collection Sites

Speleothems from the Shortwood and Netherton Tunnels were collected for analysis (Figure 19). Two stalactite samples were collected (286 m and 294 m) from an area of soda straws interspersed with several stalactites located in the center of the Shortwood tunnel (Figure 16). The paucity of large speleothems in the Shortwood tunnel allowed for the collection of only the two samples. No samples were collected from the Wast Hills Tunnel; the only calcite accumulations that were significant were associated with airshafts (Figure 17), and therefore difficult to infer the environment of formation. Several samples were collected from the Netherton Tunnel (Figure 18). Sample N5 was collected on the west wall at 1610 m, in the center section of the tunnel, from what appeared to be a stalactite, however, after sampling, it was determined that the flowstone had formed around a pipe. The rest of the samples were collected from the southwest portion of the tunnel. A second sample (N2) was collected from the continuous stretch of flowstone along the west wall at 2338 m. The thin flowstone at 2538 m yielded Sample N1 while two

samples (NB and NA) were cut from the thick flowstone of the east wall at 2559 m and 2628 m, respectively.

Speleothem Sample Collection

Rock samples from the Shortwood Tunnel were collected with a chisel and hammer. In the Netherton Tunnel, samples NA and NB were sampled with a battery-operated rock saw. It was not possible to sample the calcite accumulation to the base against the brickwork because the flowstone was slightly thicker that the cutting-depth of the rock saw. Sample N1, N2 and N5 were collected with a chisel and hammer.

Local Water Testing and Collection

Drip water samples were tested on-site with Fisherbrand pH paper for 6-8 pH range. Alkalinity was estimated with Hach AquaChek alkalinity test strips along the length of the tunnel at 150 m, 1590 m, which coincides with the location of rock sample N5, and 2325 m inside the northern entrance.

Meteoric, tunnel drip and tunnel puddle water were collected over the course of one year (February 2018 - February 2019). Samples of rainwater were collected during rain events at a residence in district B29 (Birmingham Selly Oak) close to the beginning of each event, followed by up to 3-4 samples at hourly intervals when possible.

Additionally, drip and puddle samples were collected from the Netherton Tunnel every two weeks. Drip water collection occurred from flow down the tunnel wall approximately 260m inside the south entrance at the location of the sample site NAC. Water from the puddle at the base of the wall within 1 meter of the NAC location was

collected concurrently. All of the collected water samples were stored in 15 mL plastic centrifuge tubes. The caps were wrapped in Parafilm tape for an airtight seal. The samples were stored in a refrigerator until they were bagged and shipped back to the United States. Upon arrival to the U.S., the samples were logged, prepared, and analyzed on a Picarro L2130-i Ultra High precision Isotopic Water Analyzer with an attached Picarro High Precision Vaporizer at the Large Lakes Observatory, University of Minnesota in Duluth. Results of the ^{18}O isotope values were tabulated in Excel.

Speleothem Analysis

X-ray fluorescence (XRF). Once the speleothem samples were collected, they were cut and polished to evaluate internal structure. They were first analyzed by a core-scanning ITRAX XRF at the Large Lakes Observatory at the University of Minnesota Duluth. The highest resolution of .2 mm was utilized to investigate the elemental composition of the samples. The samples were scanned from the most recent deposits to the oldest. The results were reprocessed and normalized to kilocounts per second (kcps), which can act as a measure of density. This normalization corrects for minor differences in porosity of the calcite.

Confocal microscopy. The University of Minnesota Duluth's Research Instrument Lab (RIL) used a Zeiss LSM710 Confocal Laser Scanning Microscope with a 488 nm Argon laser at 2% power and emission filter of 493-556 nm to image the samples. Numerous frames, each with a field of view of 1395 µm × 1395 µm, were patched together by a tile scan to create a total scan area, which varied in rectangular shape and included sufficient fields of views to encompass features of interest for each sample. The resolution

was 64x64 pixels of size 22.14 µm x 22.14 µm and the pixel dwell time was set to 355µsec/pixel and a frame scan rate of 2.03 sec/frame. The process used a Zeiss EC Plan - Neofluar 10x M27 (dry objective) objective lens with a focus depth from the surface of approximately 50-100µm.

Oxygen and carbon isotopes from speleothems. Select speleothems were chosen for sub-sampling and stable isotope analysis. Samples were drilled from speleothems at 1 mm intervals using a Dremmel Multi-Pro drill fitted with a 0.5 mm dental drill bit. Two transverse sections from the Netherton tunnel were submitted for preparation and ^{18}O and ^{13}C isotope analyses. The LacCore Lab at the Limnological Research Center Core Facility, University of Minnesota Twin Cities, prepared an initial batch of samples for stable isotope analysis. Bleaching, rinsing and centrifuging to decant off water served to remove organics. The samples were then shipped to the Stable Isotope Lab at Utah State University. Prepared samples were transferred into analysis vials and dried in a vacuum oven to remove all liquid. C and O isotope ratios were then analyzed on a Gasbench and Delta V IRMS using the phosphoric acid method (McCrea, 1950). The powdered carbonate is flushed with helium then acidified with approximately 100 microliters of 103% phosphoric acid for 2 hours at 50°C. A second batch was sent to Utah State for both preparation and analysis.

The carbon and oxygen delta values of the speleothem subsamples were then compared to instrument records, air quality and land use change. Statistical Analysis System (SAS) was used to run correlation and principle component analyses. Delta values were analyzed the against annual 1-yr, 2-yr, 3-yr, 4-yr, 5-yr, 6-yr, 7-yr, 8-yr and 10-yr running averages of Central England Temperature (CET), Central England Precipitation

(CEP), NAM, NAO, AMO, as well as the annual air quality and land use data pertaining to the speleothem sample year.

Determination of calcite formation in equilibrium conditions. The oxygen delta values of the meteoric water in VSMOW were first converted to PDB. The Kim & O'Neil equation [9] was applied to derive the equilibrium fractionation factor (α) for calcite for the range of tunnel temperatures, 6°C - 16°C. Using the calculated α, estimates of $CaCO_3$ $\delta^{18}O$ values were calculated for formation in isotopic equilibrium. The estimates were then compared to the actual $\delta^{18}O$ range of the calcite (Kim & O'Neil, 1997; Lachinet, 2006).

Instrument Station Data

Three sets of instrument data from the UK Met Office were gathered and analyzed: the CET, EWP and the Historical Station Data. Initially, conversion to Julian Day was necessary to handle dates prior to 1900 in Excel. With the application of our age model, inclusion of instrument station data prior to 1900 was no longer necessary. 1-year and 10-year moving averages were calculated in Excel.

Evaluation of the individual station data indicated they coincided with that of the CET, therefore only the CET record was used for the analysis. Tmin, Tmax and Tavg for both the individual and the HadCET data sets were computed for the period 1961-1990, and Tmin, Tmax and Tavg deviation from the 30-year mean were derived, from which Z-scores were calculated. The Met Office also provided a monthly precipitation record, HadUKP CEP (Alexander & Jones, 2001) from 1873-present.

Climate Indices

NAO indices (Jones et al.,1997) were retrieved from the UK's Climatic Research Unit. Hurrell's NAM dataset (Hurrell & NCAR, 2018) was obtained from the National Center from Atmospheric Research. AMO data (Trenberth & Zhang, 2019) was gathered from unsmoothed Kaplan SST V2 detrended and maintained by NOAA's Earth System Research Laboratory.

For CET, CEP, NAM, NAO and AMO, the cold season and warm season of each, the 1-year, 2-year, 3-year, 4-year, 5-year, 6-year, 7-year, 8-year and 10-year running averages were calculated.

Air Quality

Mooers et al. (2016) reconstructed air quality for the period 1890 – 2010 based on gravestone weathering. Gravestone weathering is a direct measure of acid deposition and was calculated at 10-year intervals. These data are used as an environmental proxy for air quality.

Land Use

Land use changes were derived from a time series of historical Old World Maps dating from 1904, 1921, 1938, and Google Earth Imagery from 1945, 1998 and 2017. In the immediate vicinity of the Netherton Tunnel, the percentage of farm, industrial and residential land was determined for each period.

Dating - An Age Model

The commonly used radiometric dating methods were unavailable to determine the chronology of the tunnel speleothems. U-Th dating was not an option since the U content

could not be verified. Additionally, after acidification of Netherton Tunnel samples with HCl (Konitzer et al, 2012) a slight residue remained indicating the presence of trace amounts of organic matter. The U-series dating lab could not analyze the samples, as the organics would be in the same mass range as thorium, and potentially foul the Thermal Ionization Mass Spectrometry (TIMS) equipment. The ^{210}Pb method requires 5-8 half-lives to arrive at a depth where ^{210}Pb is unsupported and the tunnel is not of sufficient age. Additionally, the ^{210}Pb dating depends on high ^{226}Ra content and no detrital ^{210}Pb, which could not be verified.

Speleothem growth is gradual and distinct layers of annual deposition can often be analyzed. Therefore, and age model was developed based on a three-stage approach. First, confocal microscopy was used to identify organic matter layering, which were then counted manually in both Photoshop and Image J (Figure Confocal NAC, N5, NB1). Second, thin sections were prepared by Texas Petrographic Services and viewed with cross polarization on a Leica DMLP/Canon EOS System/Apple Computer petrographic microscope. Rock crystals were identified by extinction under cross-polarized light, by color variations with adjacent crystals, or both (Figure 14). Using a micrometer grid, the individual crystal layers were measured and totaled.

In the third approach, the Sr/Ca ratio was plotted and fitted with a spline curve in R-Spec astronomical software to smooth the data to highlight peaks. R-spec was designed for smoothing emission and absorption lines from stellar spectra, an application that is well suited for geochemical data. The procedure allows parameterization of the spline fit that can affect the recognition of small peaks. Therefore, three settings were used for low,

medium, and high filter. To obtain an objective result, the average tally for each of the three levels was calculated. The peaks were also counted manually as a check on the automated count.

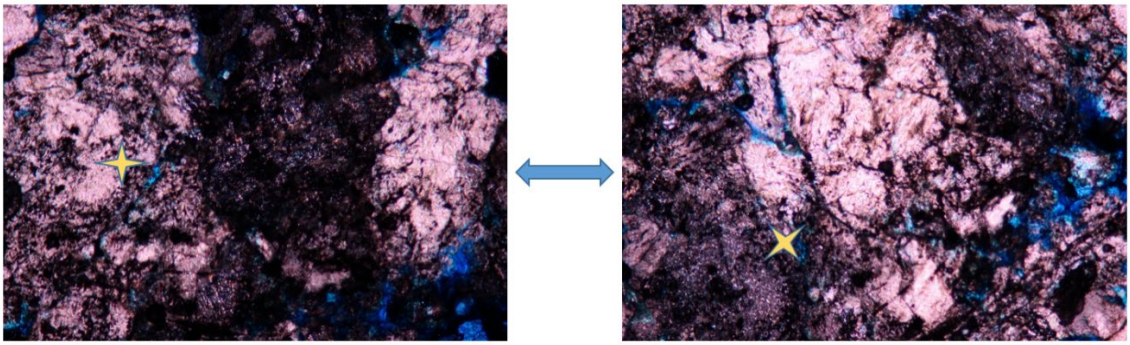

Figure 14. Rock crystals under cross-polarized light of petrographic microscope

The commonly used radiometric dating methods were unavailable to determine the chronology of the tunnel speleothems. U-Th dating was not an option since the U content could not be verified. Additionally, after acidification of Netherton Tunnel samples with HCl (Konitzer et al, 2012) a slight residue remained indicating the presence of trace amounts of organic matter. The U-series dating lab could not analyze the samples, as the organics would be in the same mass range as thorium, and potentially foul the Thermal Ionization Mass Spectrometry (TIMS) equipment. The ^{210}Pb method was omitted as the analysis requires 5-8 half-lives to arrive at a depth where ^{210}Pb is unsupported and the tunnel is not that old. Additionally, the ^{210}Pb dating depends on high ^{226}Ra content and no detrital ^{210}Pb, which could not be verified.

The ^{14}C content was analyzed by Accelerated Mass Spectrometry at International Chemical Analysis Inc., Ft. Lauderdale, Florida, to search for an increase in ^{14}C associated with bomb carbon. Four samples across the axis of growth were processed for radiometric

dating and determination of percent modern carbon in an effort to identify the presence of atmospheric testing bomb carbon.

Local Hydrology

The isotopic composition of precipitation events provided data to create a local meteoric water line (LMWL) that displays the relationship of ^{2}H and ^{18}O in meteoric waters. Isotopic analysis and the comparison of delta values of drip water and local precipitation were then used to evaluate residence time of infiltrating water through the vadose zone (Lachinet, 2006, Kendall & McDonnell, 1998, Turner & Barnes, 1998).

Geology

ESRI's ArcMap was used to perform Geographic Information System (GIS) analysis of the study site. 1:50,000 scale geologic maps (British Geological Survey) and Shuttle Radar Topography Mission (SRTM) elevation data served as the base map. Canal locations and land use layers derived from Google Earth were overlain onto the base. Borehole data from the vicinity of the tunnels were digitized. Geologic cross-sections were created from borehole data using Strater© software from Golden Software, Inc. Faults and fractures were added from digitized geological maps. GIS maps and the log records were used to create tunnel and tunnel events shapefiles.

Results

Speleothem Mapping

The Shortwood, Wast Hills, and Netherton Tunnels exhibit different speleothem characteristics and abundance. Speleothem locations in the tunnels reflect the presence of

fractures or faults in the overlying strata. In the Shortwood tunnel, the most substantial speleothem growth occurs at the southwest end where a fault crosses the tunnel (Figures 8 and 16). Wast Hills tunnel is nearly devoid of speleothems (Figure 17); Figure 8 shows that no significant geological structures are present. The Shortwood tunnel is overlain by Mercia Mudstone Group, which is extremely homogeneous and devoid of structures.

Netherton Tunnel, in contrast, has substantial speleothem growth at several locations. Figures 8 and 9 illustrate the geology and geological structures associated with the Etruria Formation and Middle Coal Measures that overlie the tunnel. The presence of faults and fractures in the center of the tunnel and within a few 100 meters of its southwest entrance are associated with the most well-developed speleothems. Specific descriptions and interpretations for each tunnel follow in order of mapping: Shortwood, West Hills, and Netherton. Distance markers are relative to the side of the tunnel entered for mapping. For example, the Shortwood Tunnel was entered from the northeast so reference point 0 m is at the northeast tunnel entrance. At the time of mapping, all speleothems were assumed to be composed of calcite minerals.

The Shortwood Tunnel, south of Birmingham on the Worcester and Birmingham Canal, is approximately 560 m long and consists of the original brick tunnel alternating with refurbished sections of concrete lining. Overall, speleothem formation in the Shortwood Tunnel is patchy and consists mainly of soda straws and poorly formed, small stalactites (Figure 15). From the northeast, the Shortwood Tunnel is structurally reinforced with concrete for 40 m, and speleothems are thin or poorly developed. The northeast end contains a short section (~10m) of sparse soda straw formations (40-48 m). The remainder

of the northeast half of the tunnel is barren of calcite deposits. Heavy drip, evidenced by running or rapidly dripping water, occurs in the southwestern center of the tunnel at 353 m and 378 m. A patch of soda straws (394 m) is followed by thin flowstone (431 m). At 440 m, soda straws evolve into a soda straw garden. A large speleothem formation at 450 m consists of calcite formed about an oxidized pipe. A second soda straw garden spans from 470 m to 483 m, although few soda straws persist. A combination of soda straws and flowstone exists at 491 m. Flowstone alone occurs at 529 m. No formations exist along the 33 m remaining to the southwest exit.

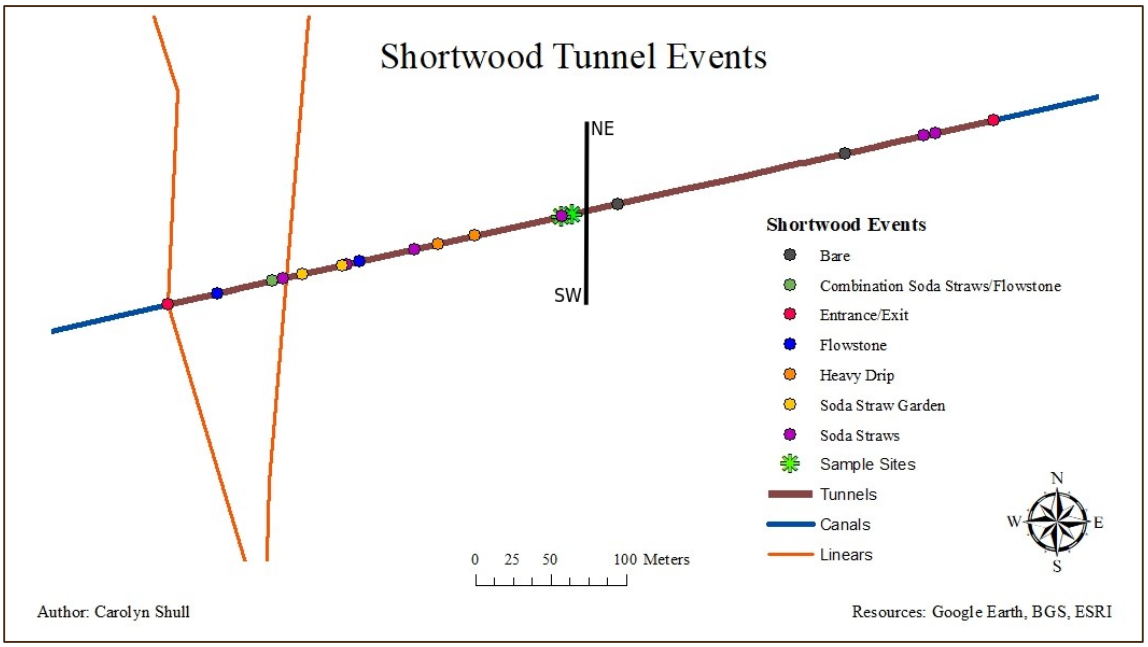

Figure 15. Shortwood Tunnel Events

The **Wast Hills Tunnel**, is one of the longer tunnels in the canal system (Cumberlidge, 2009). The tunnel, however, contains minimal speleothem growth (Figure 16). Three airshaft vents are dispersed along the length of Wast Hills Tunnel, and calcite formations created by a constant flow of water at the vents, though substantial, was not

sampled. Water seepage responsible for the formation of the calcite deposits appeared to come largely from seepage around the margins of the airshaft's steel lining. They were considered to be influenced almost entirely by the air vent and not typical of other speleothems. From the southern entrance, the tunnel contains dripping water (17 m) and a mix of thin flowstone and soda straws (34 m). A bare stretch for 84 m in the southwest section of the tunnel begins a pattern of sparse events. Dripping water (118 m), flowstone (169 m and 278 m), heavy drip water (451 m) and an area containing a mixture of rapidly dripping water, soda straws and flowstone (747 m) are the next features with an expanse of tunnel between each (51 m, 110 m, 173 m, 295 m respectively). After another 139 m with no events, drip (886 m) and flowstone (924 m) occur. Flowstone (1186) is present again 262 m further to the north. In the northeast portion of the Wast Hills tunnel, three consecutive regions of combined soda straws and flowstone are located at 1312 m, 1326 m and 1422 m. Seven events of thin flowstone are evident at intervals of 10-41 m, with heavy drip within 7 m of the fifth flowstone event. Flowstone and heavy drip (1733 m), drip alone (1870 m) and flowstone and drip (1941 m) punctuate the tunnel continuing north. Two areas with soda straws (2083 m and 2258 m) occur approaching the northern exit.

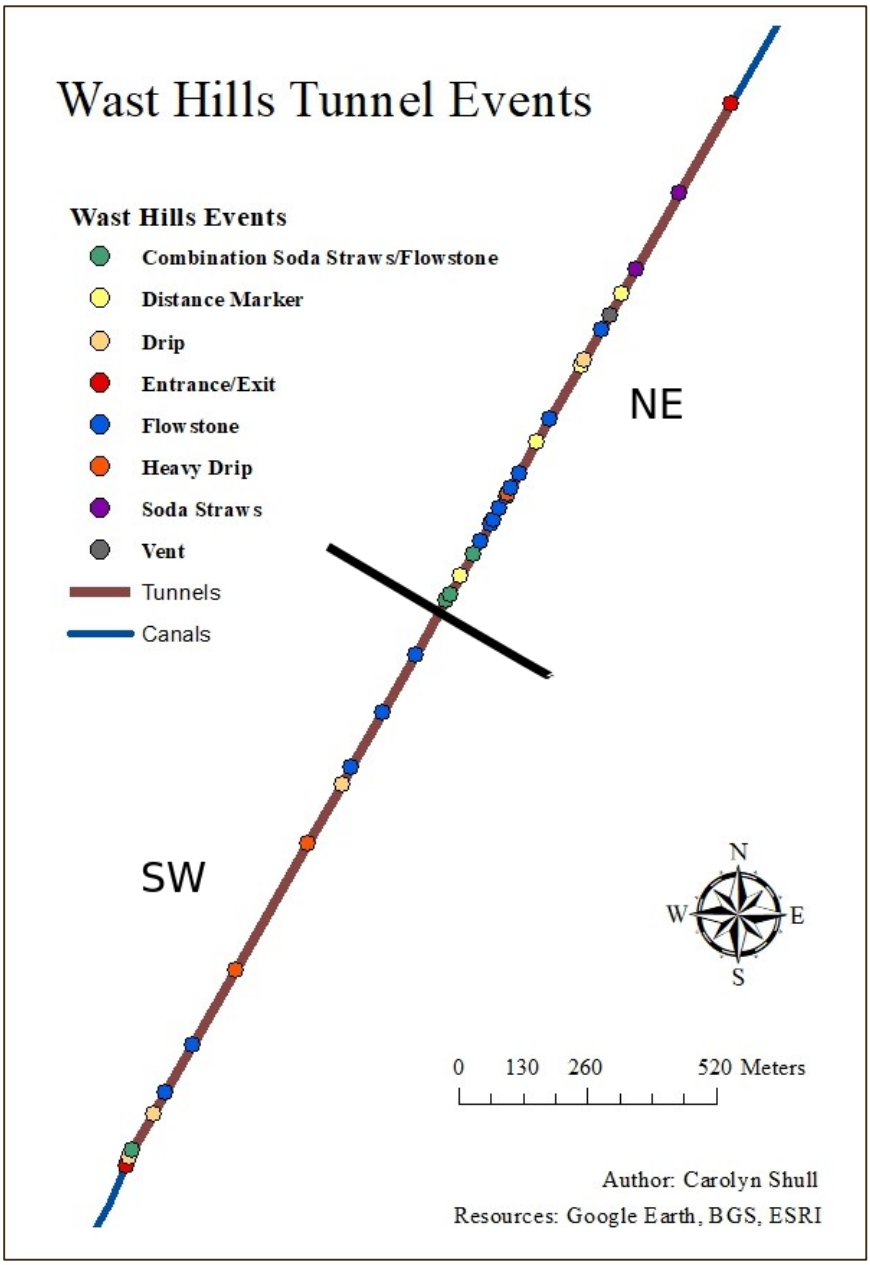

Figure 16. Wast Hills Tunnel Events

The **Netherton Tunnel**, is characterized by frequent areas of dripping or running water and extensive speleothem growth (Figure 17). In the northeast section, small drips occur at 68 m, 81 m, and 154 m. Small or thin amounts of flowstone are located at 109 m and 199 m. Heavy drip is encountered at 349 m. Thin flowstone and flow ribbons occur

between 419 m and 457 m. Flowstones bands form at 500 m and 516 m. A small patch of flowstone at 605 m is followed by natural brickwork for over 200 m. Heavy drip (842 m) is followed closely by flowstone (851 m). Approaching the center section of the Netherton Tunnel, two small separate areas of flowstone are located at 903 m and 967 m. Flowstone does not form again until well into the center of the tunnel at 1202 m with drip nearby at 1207. Flowstone and heavy drip simultaneously occur at 1277 m. Additional flowstone forms down-tunnel 100 m at the very center of the tunnel (1380 m). A refurbished area, consisting of concrete lining, marks the tunnel at 1446 m. Thin flowstone covers the walls at 1499 m and thickens into flowstone at 1520 m. Soda straws form amid flowstone (1538 m) and a flowstone ridge on the west (right) wall mid-tunnel at approximately 1610 m had formed around a pipe, explaining the ridge. No speleothem features are located for over 200 m prior to exiting the center portion of the Netherton Tunnel. Entering the southwest section, various flowstones dominate. Bands of flowstone (1849 m and 1861 m) are followed by flowstone (1903 m, 2128 m) and flowstone with heavy drip (1918 m, 2201). Soda straws appear independently (2265 m at 2292 m) and combined with flowstone (2276 m, 2292 m, 2352 m, 2352 m). Thick flowstone of greater than 10 cm of deposited calcite (2312 m) is succeeded by a continuous stretch of flowstone (2338 m). After approximately 190 m of minimal speleothem activity, thin flowstone (2538 m) transitions to multiple sections of thick flowstone (2559 m and 2628 m), especially along the east wall. Regular flowstone is interspersed along the east wall (2577 m and 2648 m) and then both sides of the tunnel (2704 m) within 64 m of the southwest exit. Heavy drip is associated with five of the seven vents along the length of the Netherton Tunnel.

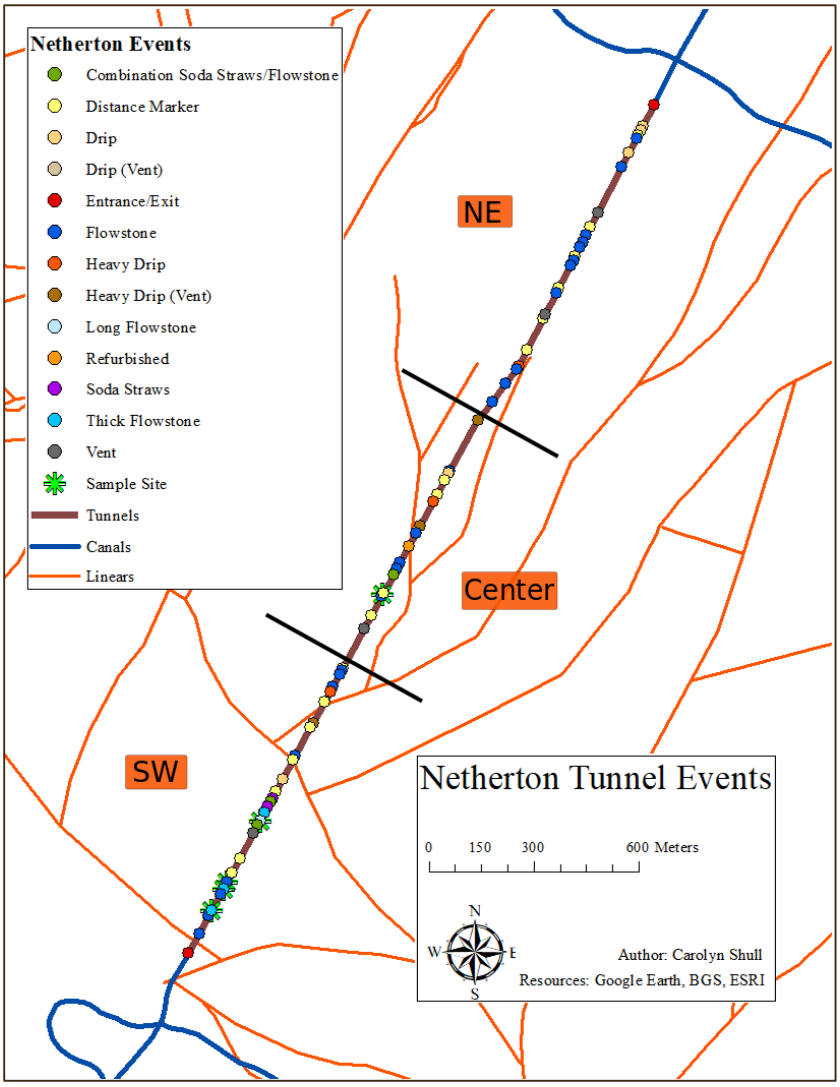

Figure 17. Netherton Tunnel Events

Tunnel Drip Water Chemistry

The tunnel drip water is circum-neutral with a pH range of 7-7.5 and alkalinities of 210-240 meq/L.

Figure 18. Prepared Speleothem samples

X-Ray Fluorescence

Based on their limited scatter and potential trends within the individual samples, sulfur, chloride, iron and strontium were considered as potential elements of interest. Concentrations of these elements were relatively constant from the most recent to the oldest depositional layers (Figure 19). No significant results or trends were consistent upon further analysis across all samples of sulfur, chloride and iron.

Figure 19. XRF Lineup of Samples. Scan started from the most recent and proceeded toward the oldest deposits

Figures 20 shows the concentration of Sr compared to Ca in the NAC sample. Figure 21 is a plot of the Sr/Ca ratio vs. position along sample NAC and Figure 22 is the splined Sr/Ca ratio as a function of position. The number of peaks in the Sr/Ca ratio was determined for each of the three spline options (low, med, high) (Table 1) by determining the slope of the curve at each position. A change from positive to negative slope corresponded to the peaks. Counts of the peaks were used to determine the age model.

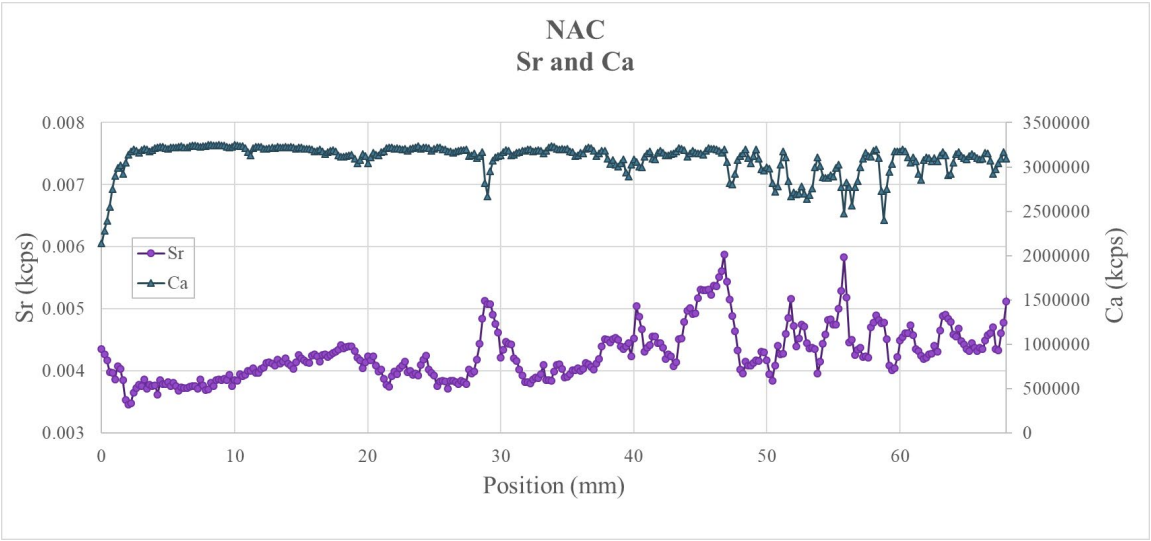

Figure 20. Sr and Ca. Note the extreme difference in scale and the mirroring that occurs.

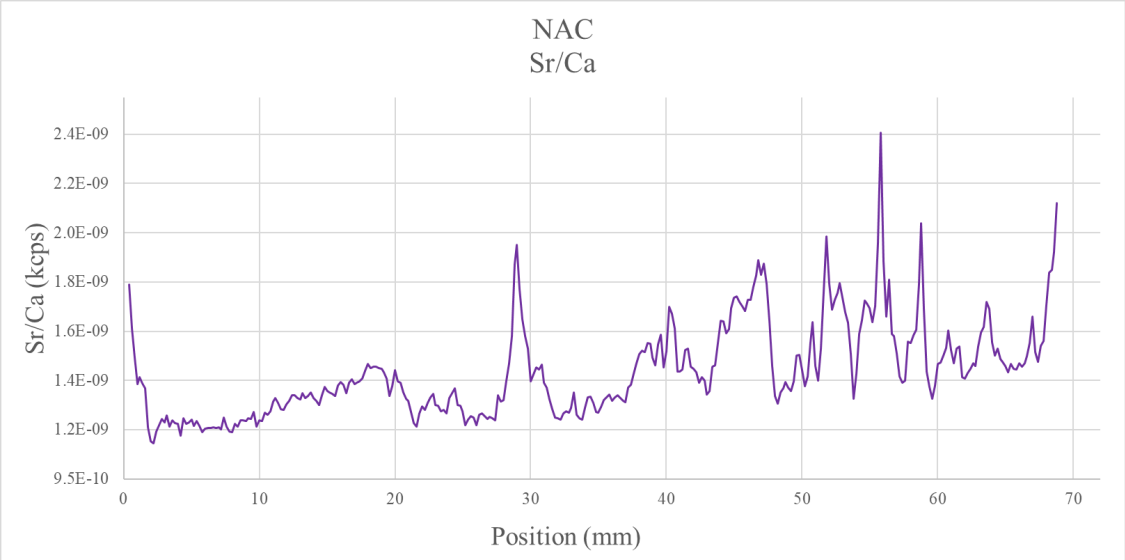

Figure 21. Sr/Ca of Sample NAC

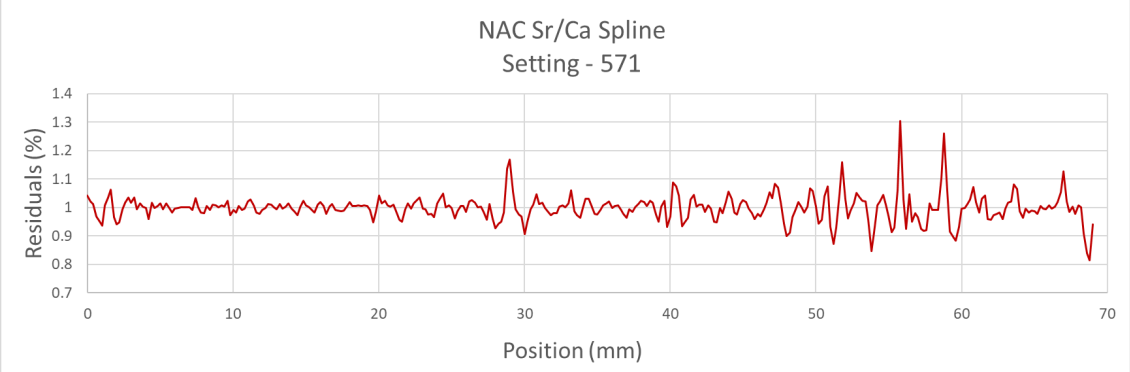

Figure 22. Sr/Ca Splined in R-Spec – Level 571 (high)

Table 1. Peak Counts at three R-Spec Spline Levels

Manual	Spline 148	Spline 550	Spline 571
87	98	88	84
Average			90

Confocal Microscopy

Samples were imaged with confocal microscope to highlight organic material within layers of each sample and provide a subjective method of determining and counting layers. Generated counts for sample NAC ranged from approximately 92 -100 couplets (Figure 23), the N5 sample (collected from a pipe) consisted of roughly 65 couplets (Figure 24), and the count for NB1 was 82 couplets (Figure 25). The reason for the discrepancy between counts is related to the interpretation of the banding. Each sample was counted three times with an interval of at least a day between counts.

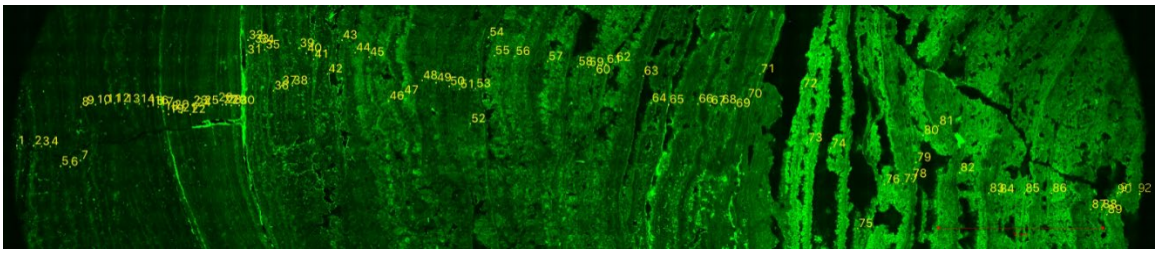

Figure 23. NAC Count - 92

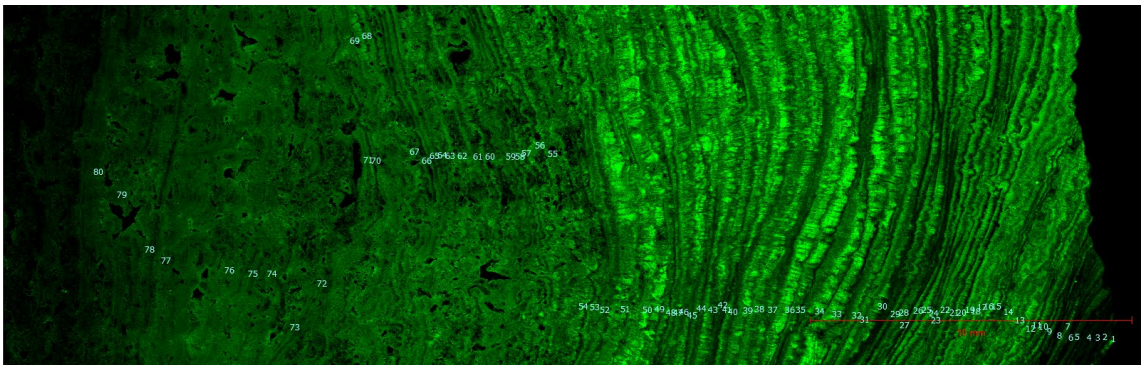

Figure 24. N1a Count - 80

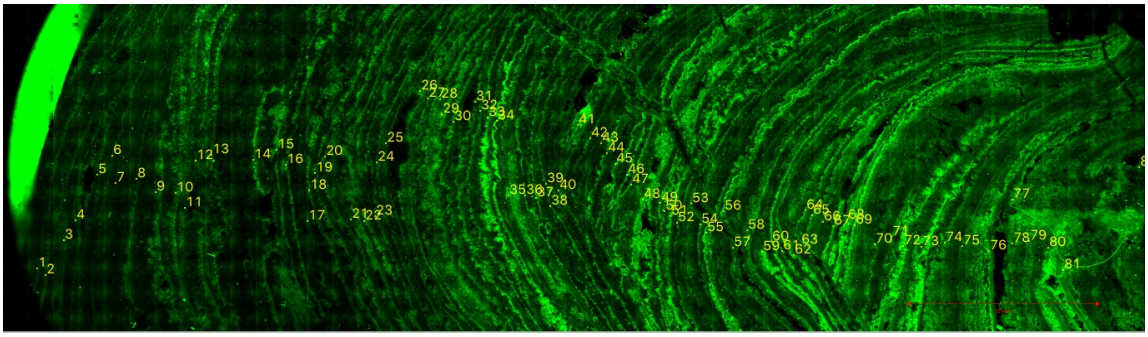

Figure 25. NB1 Count - 82

Petrographic Microscopy and Trace Element Analyses

The petrographic microscope rock crystal analysis resulted in a count of 91 layers. The R-Spec approach to the Sr/Ca peaks analysis resulted in a count of 90 layers, while the manual method outcome was 91 layers.

Age Model

The results of confocal, petrographic and Sr/Ca analyses provided the basis of an age model. Age of the annual layers was identified by year starting from the outer lamina at the time of collection in 2016. The running total of measured widths and their associated year of deposition were used to determine an age/position (mm) along the growth axis of the speleothem. Interpolating dates for each increment accounted for the varying thickness of each layer width. This timeline was then used as a catalog for the speleothem isotope dates based on sampling position.

Local Hydrology

Figure 26 is a plot of δD versus $\delta^{18}O$ for rainwater, tunnel drip, and tunnel puddle water with reference to the Global Meteoric Water Line (GMWL). Isotopic values of local precipitation describe the Local Meteoric Water Line.

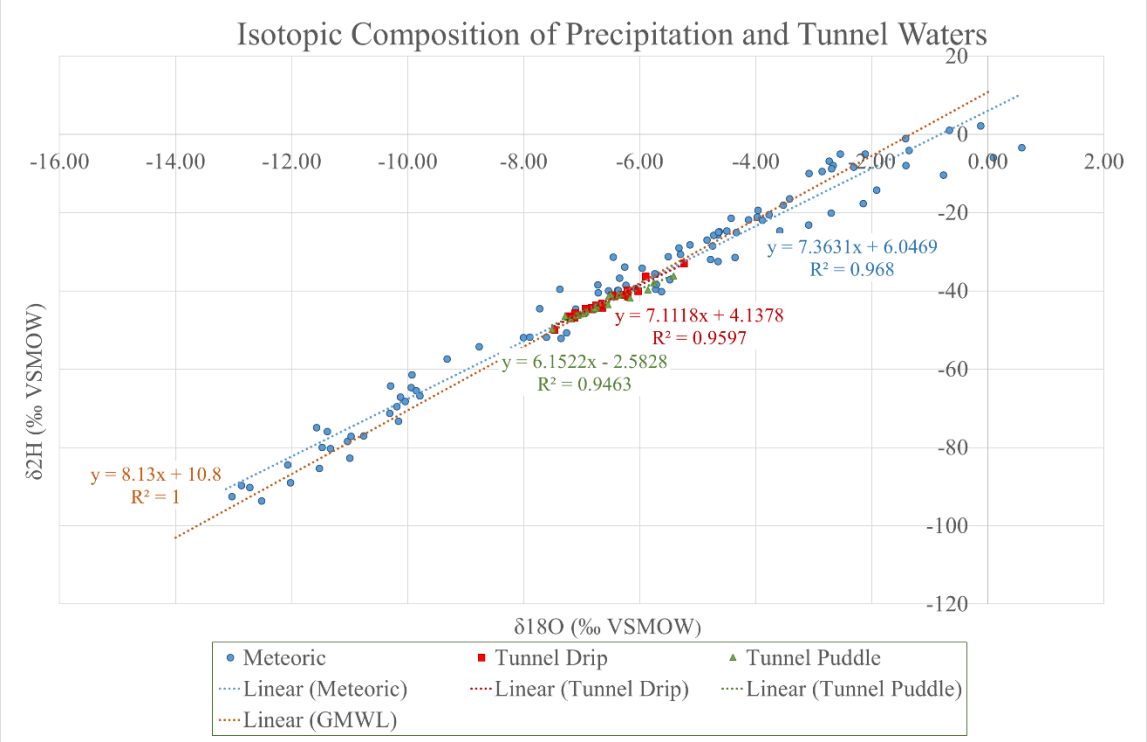

Figure 26. Isotopic Composition of Precipitation and Tunnel Waters

Tunnel drip water and puddle water plot on the local meteoric water line but have a much narrower range of isotope values than that of local precipitation. The narrow range is interpreted as mixing of the annual range of precipitation infiltrating through the vadose zone. Figure 27 displays the annual variability of isotopic composition of local meteoric water and its seasonal cycle. The vertical grouping of sample analyses reflects the change in the isotope sequence during single rain events, which is a result of Rayleigh fractionation (Clark & Fritz, 1997; Sharp, 2017). Figure 28 shows the same annual data normalized to

air temperature. Normalization smooths out much of the variability from isotopic dependency on temperature.

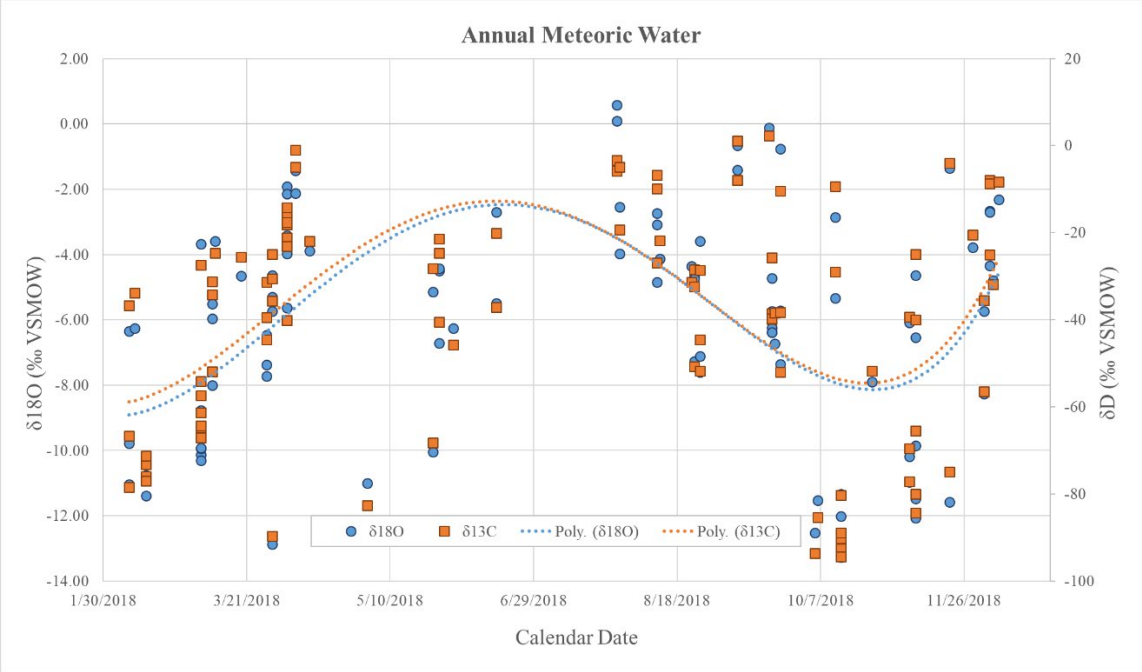

Figure 27. Annual Meteoric Water

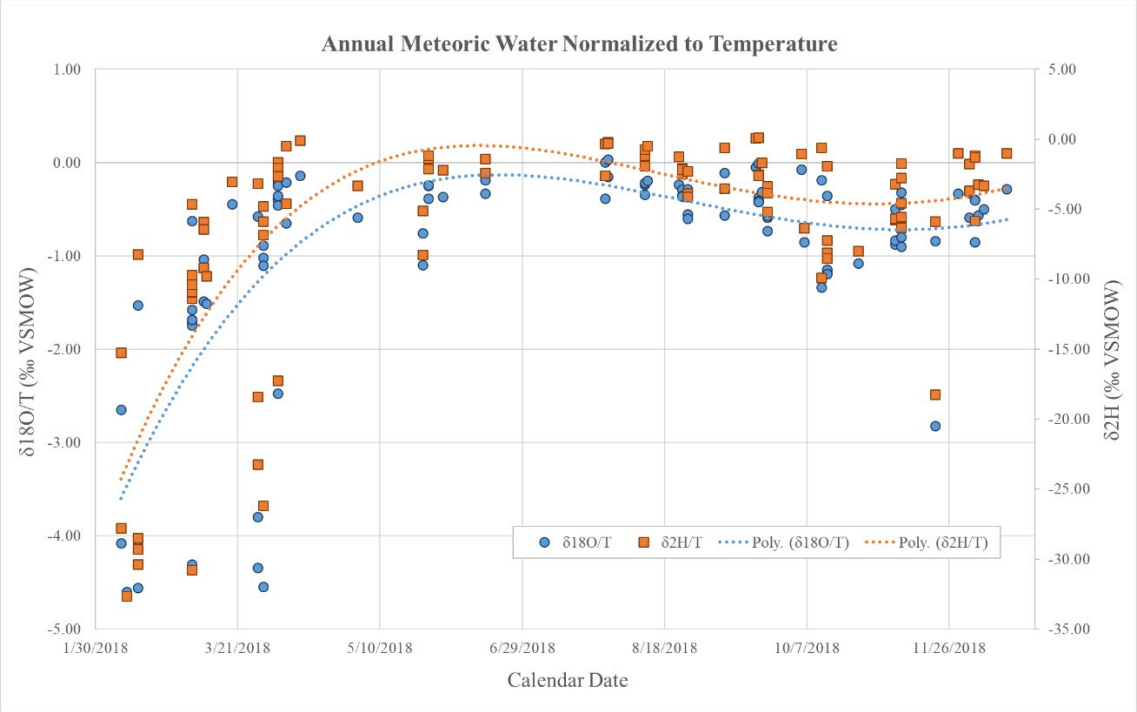

Figure 28. Meteoric Water Normalized to Temperature

Figures 30 - 33 are quarterly delta value trends in the meteoric events by month relative to those of tunnel drip and puddle water. The δD and $\delta^{18}O$ are plotted to reflect the shift in values over the course of the year. The month of the meteoric events are categorized symbolically. Note multiple rain samples collected over time from the same meteoric event are included and are not differentiated on the graphs. Some of the migration of delta values within the same month, therefore, is likely a function of Rayleigh distillation.

The seasonal shift in isotopes is evident (Figures 29 and Figure 30) as the majority of February rain events fall along the lower, left-hand reach of the LMWL where lower values for $\delta^{18}O$ and $\delta^{2}H$ lie. March and April rain events are more enriched in heavier isotopes reflecting warmer temperatures. The delta values for April rain events plot along the upper right-hand section of the LMWL where the least negative delta values are located.

The other quarterly graphs also display the migration of values along the LMWL in response to seasonal temperatures (Figures 31-33).

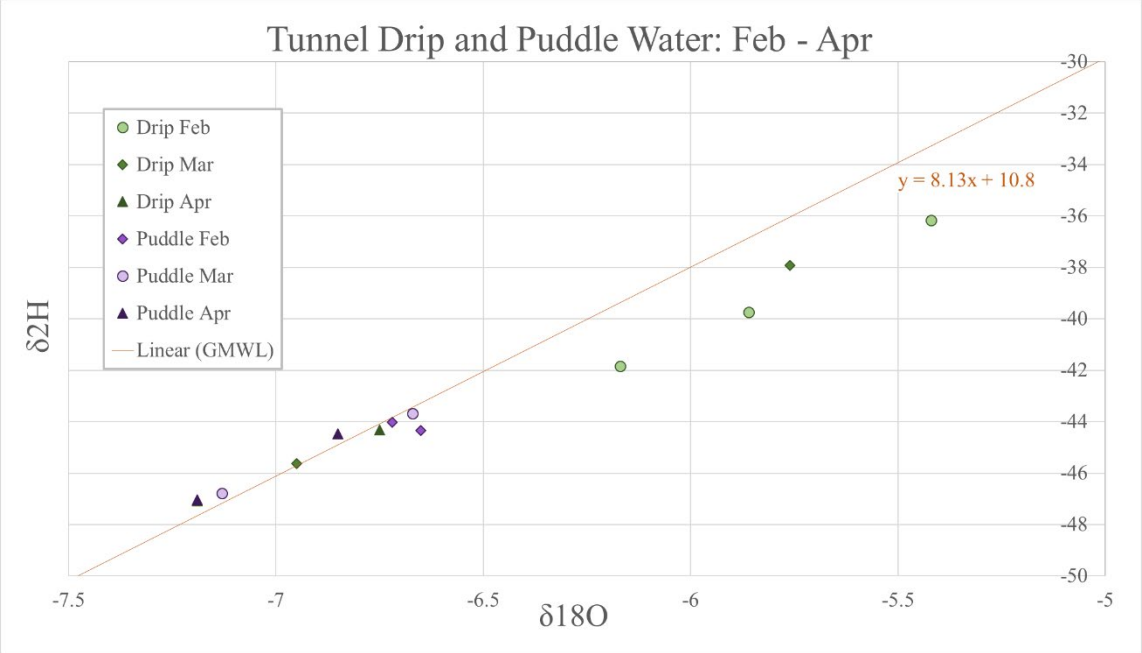

Figure 29. Tunnel Drip and Puddle Water: February – April

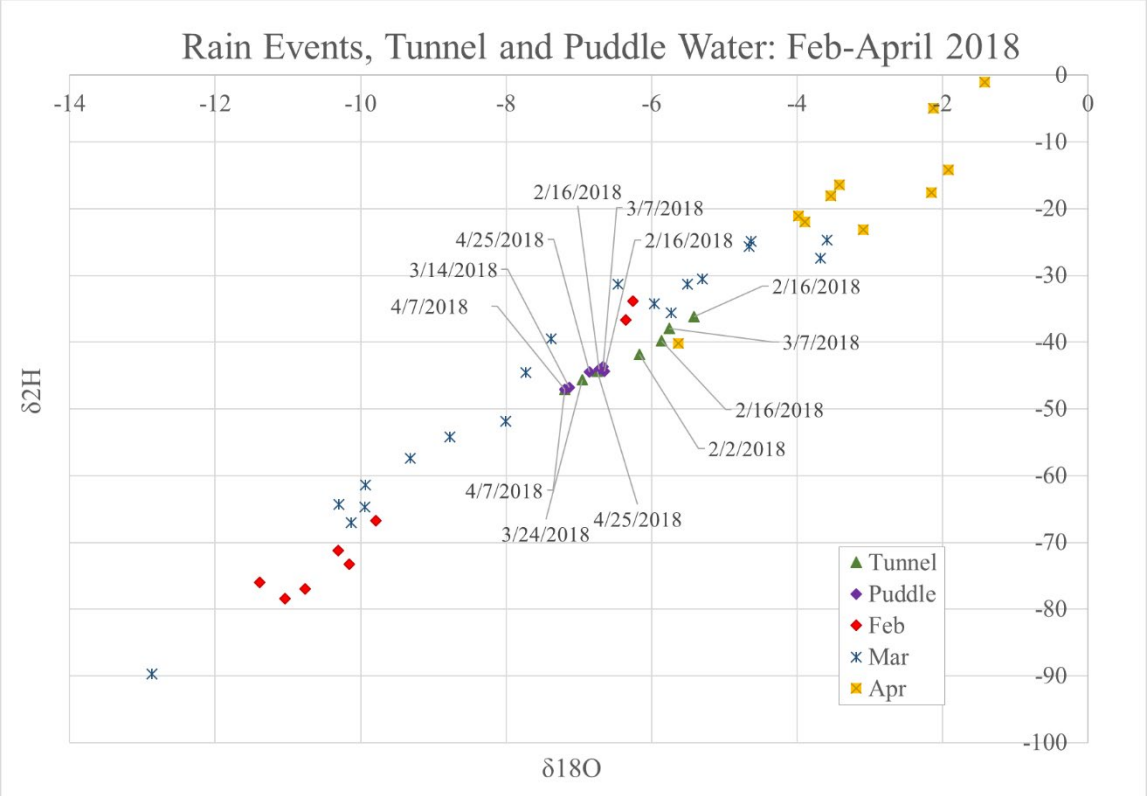

Figure 30. Rain Events, Tunnel and Puddle Water: February - April 2018

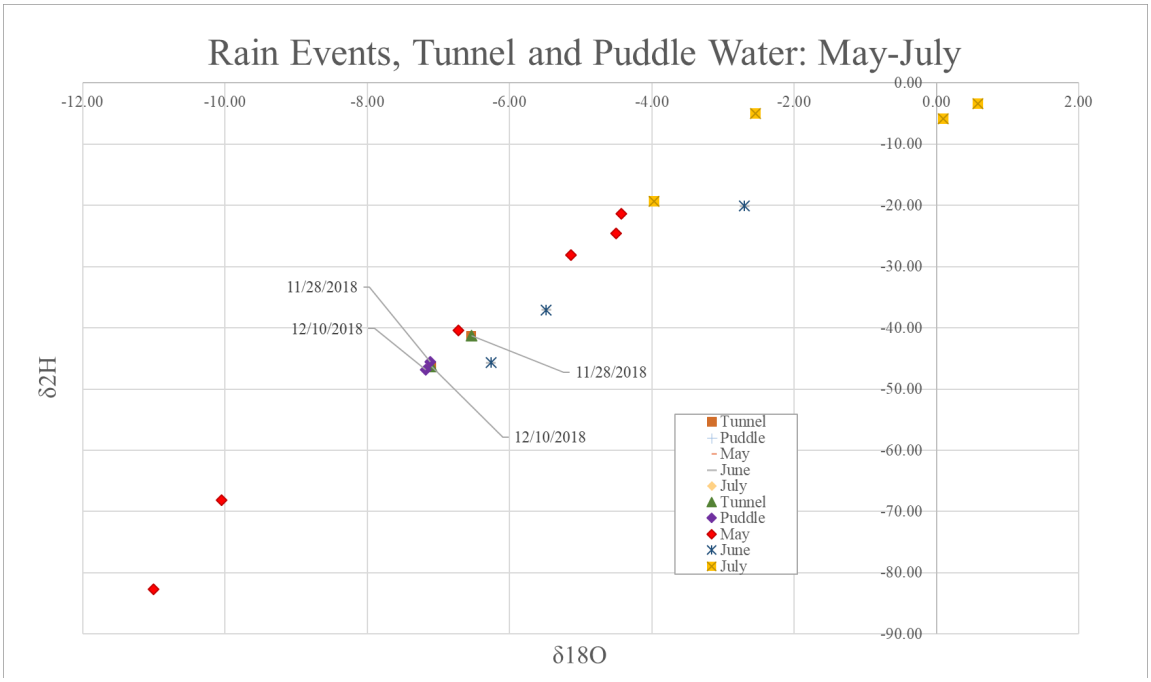

Figure 31. Rain Events, Tunnel and Puddle Water: May - July 2018

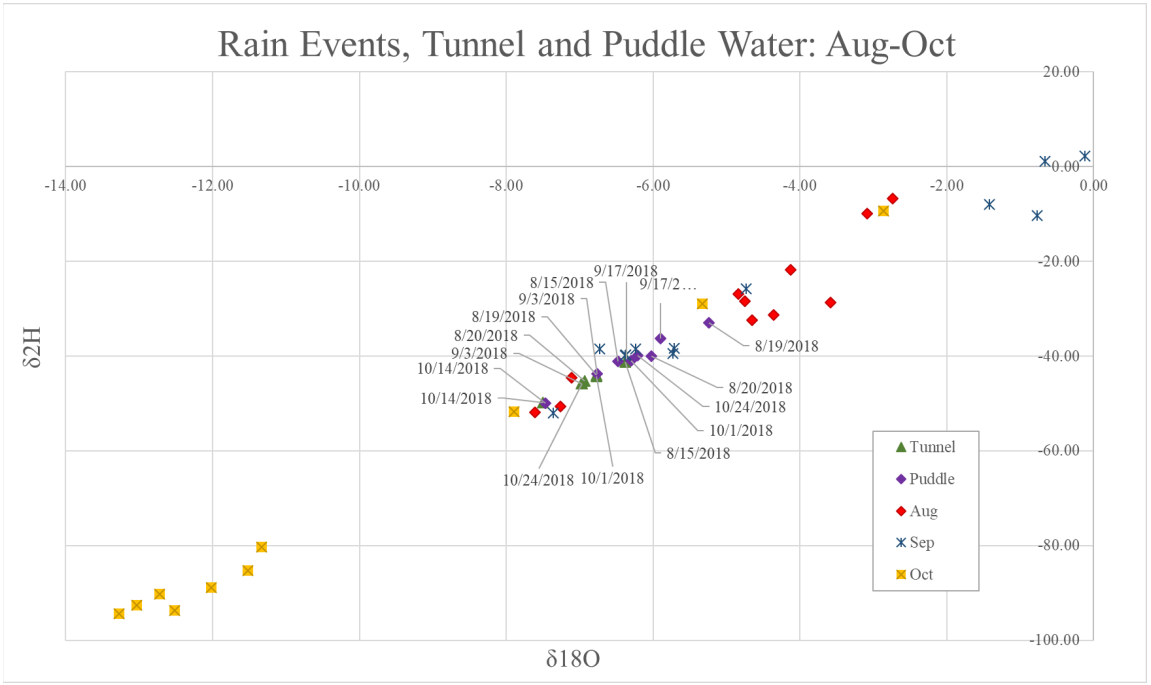

Figure 32. Rain Events, Tunnel and Puddle Water: August - October 2018

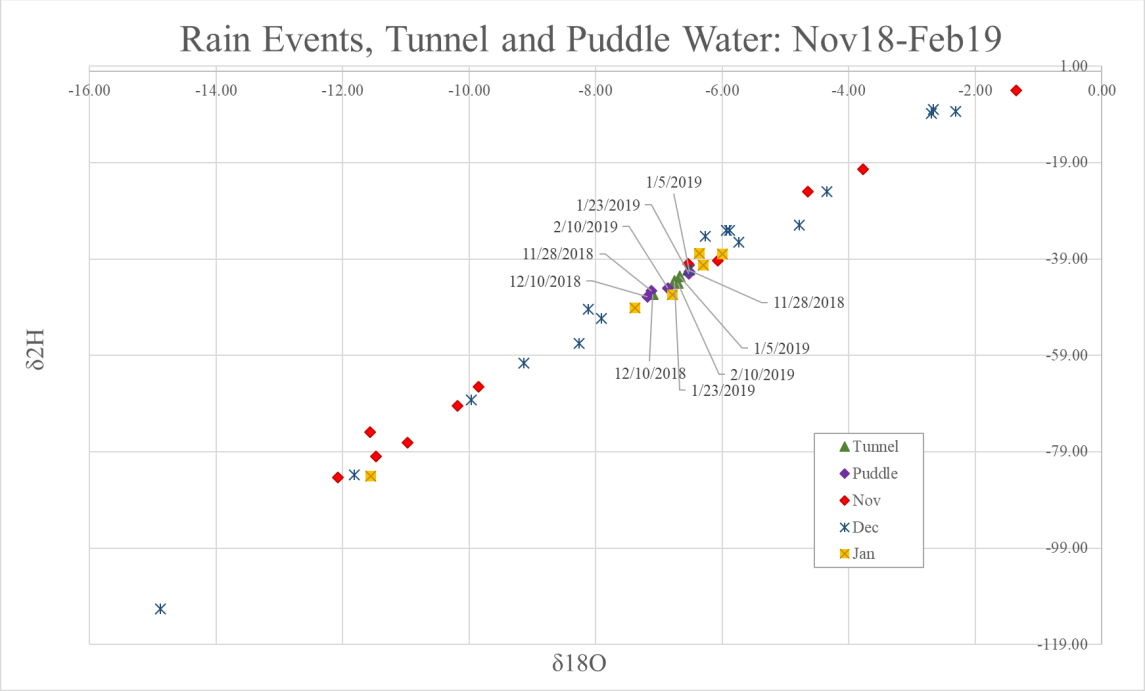

Figure 33. Rain Events, Tunnel and Puddle Water: November 2018 - January 2019

The isotopic composition of tunnel drip water is shifted by a significant amount of time, possibly 6-8 months, from surface precipitation, which is interpreted as the residence time of groundwater in the vadose zone. Figure 34 displays the variation of tunnel drip water isotope values by month of collection. Figure 35 displays the migration of the tunnel puddle water delta values over time.

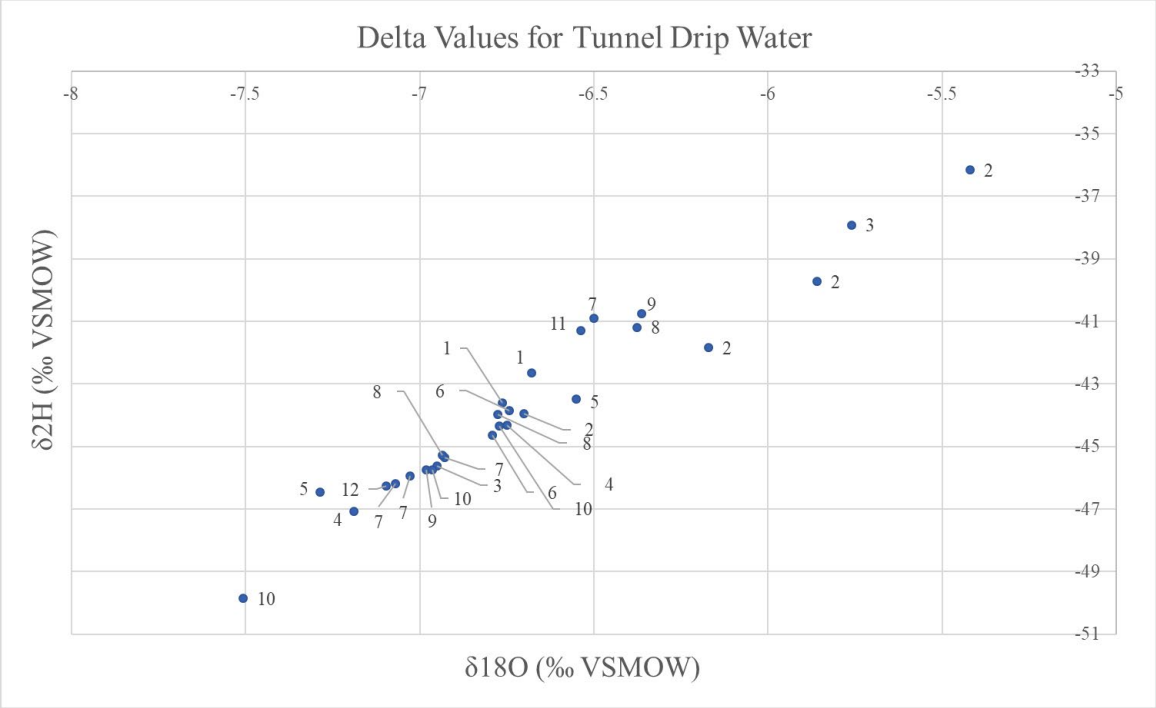

Figure 34. Delta Values for Tunnel Drip Water. The month in which the sample was collected is in numerical form adjacent to the plotted point, e.g. 10 is next to the bottom left point indicates the sample was collected in October.

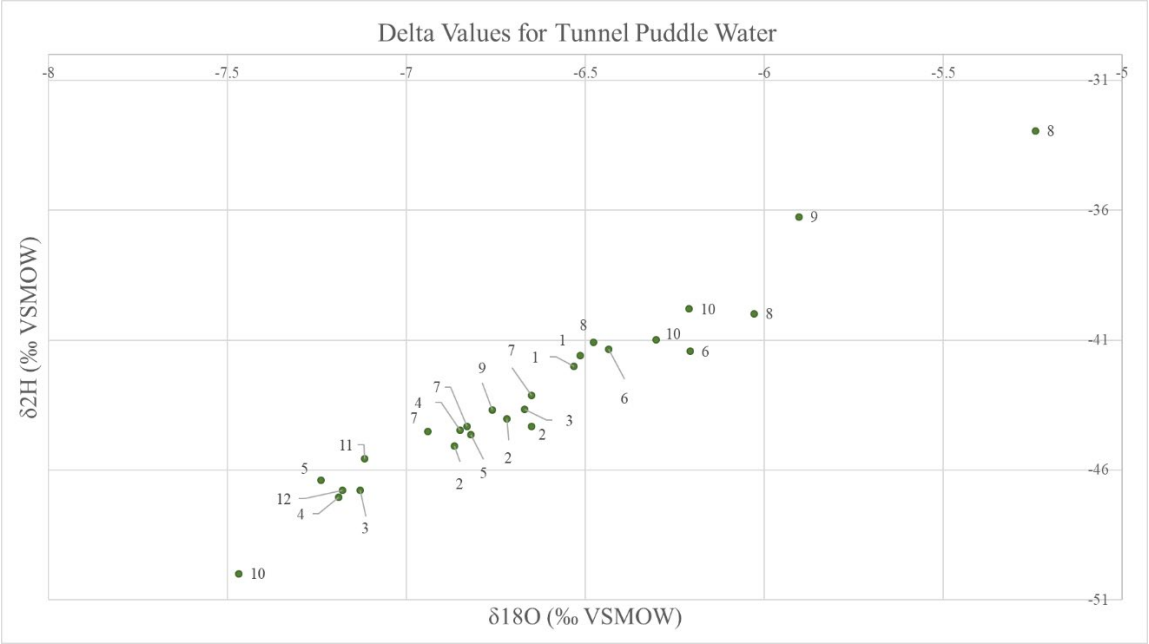

Figure 35. Delta Values for Tunnel Puddle Water. The month in which the sample was collected is in numerical form adjacent to the plotted point.

Instrument Station Temperature

Central England Temperature Record (CET). Figure 36 shows the average deviation of the annual average Central England Temperature from the 1961-1990 climate mean. The warming trend over the last few decades is consistent with other long-term temperature records from the UK and Europe (Benner, 1999; Hughes, 2000).

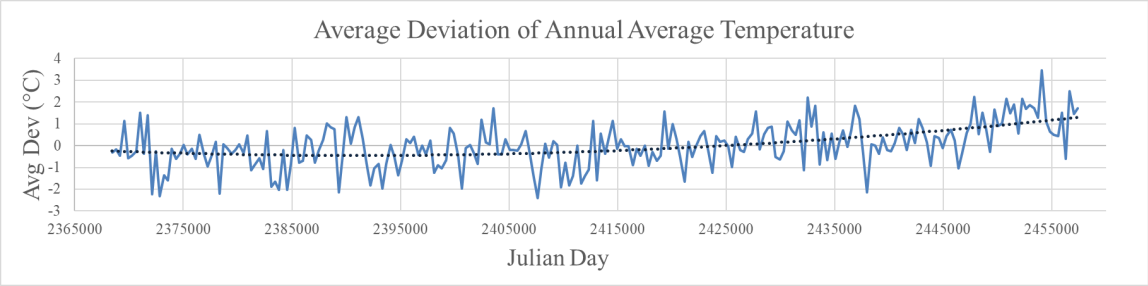

Figure 36. Central England Temperature

Individual Station Data. The data from Edgebaston, Shawbury, Sutton Bonnington and Oxford, several of the temperature records used to compile the CET, are shown in Figure 37 and Figures 39-41. Analysis of these four temperature records shows essentially the same pattern of increasing temperatures since the late 1970s. From 2000-2012, the deviation remained predominantly positive. The 20-year gap in the data at Edgebaston is unfortunate (Figure 37 and Figure 38) but actually emphasizes the 0.15-0.2 unit increase in the z-score.

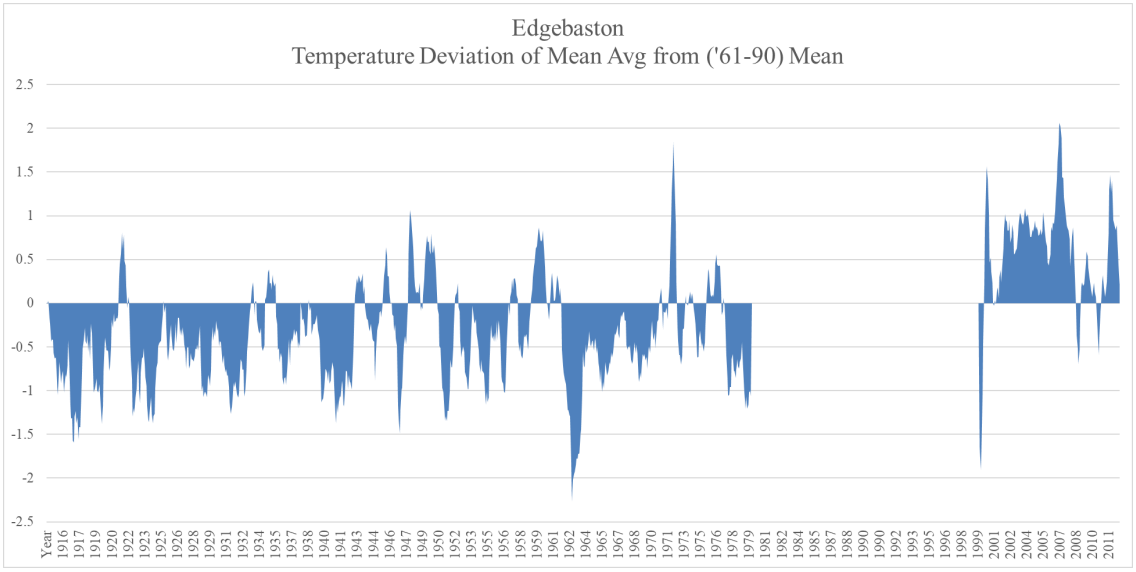

Figure 37. Edgebaston Temperatures. Comparison of the deviation of the 12-month moving average temperature from the temperature mean for the 30-year climate period between 1961 and 1990 for Edgebaston.

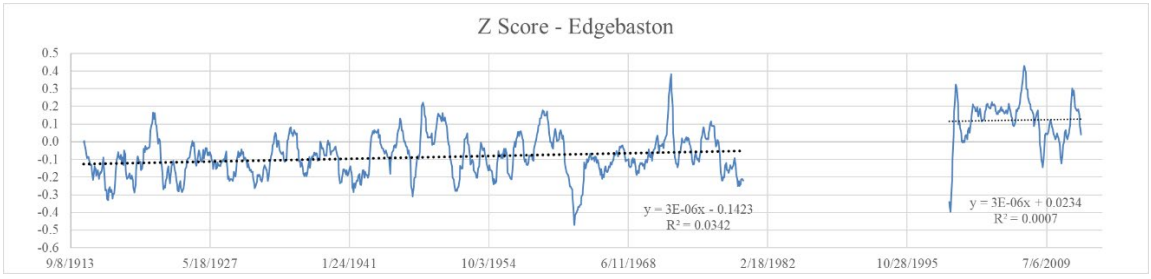

Figure 38. Z-Score Edgebaston

The remaining individual station data reflect the change of the mean temperature averages from a predominantly negative to a generally positive deviation around 1990 relative to the 1961-1990 mean (Figures 39-41).

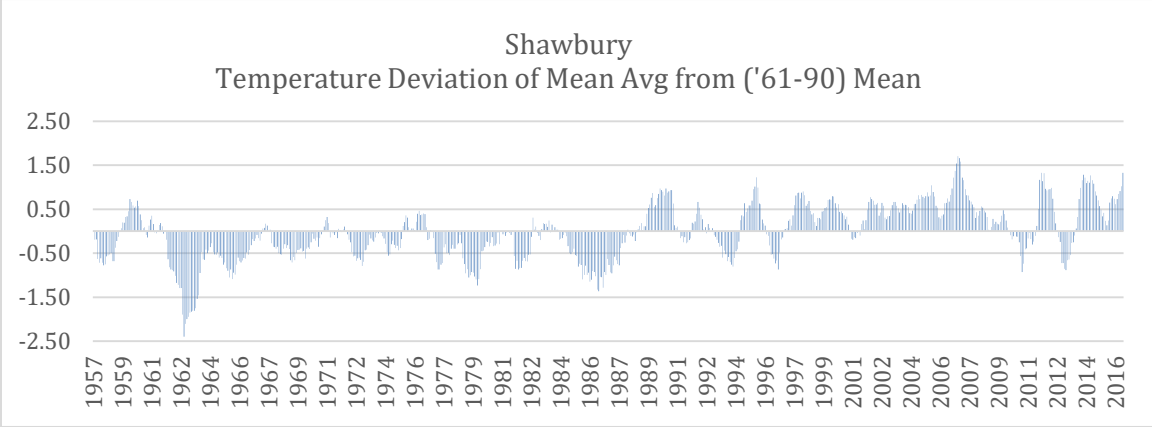

Figure 39. Shawbury Temperatures. Comparison of the deviation of the 12-month moving average temperature from the temperature mean for the 30-year climate period between 1961 and 1990 for Shawbury.

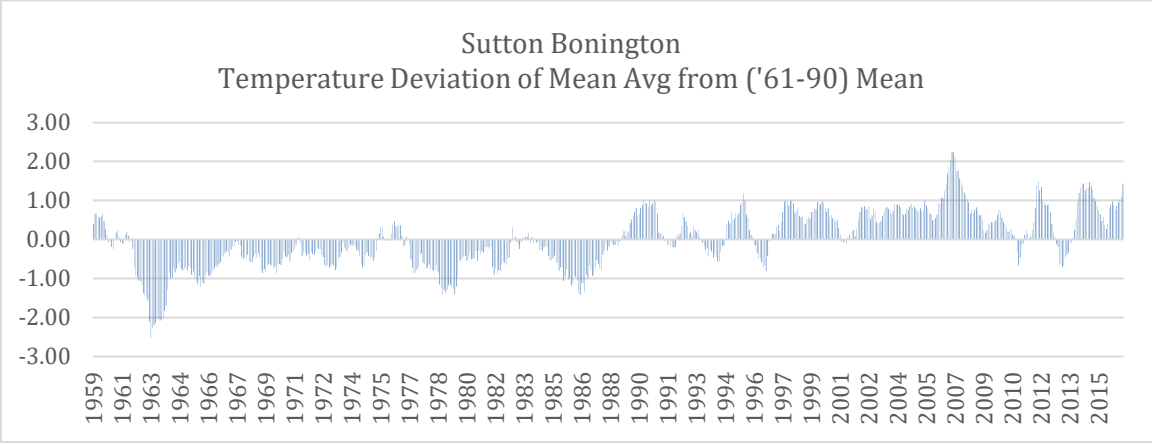

Figure 40. Sutton Bonington Temperatures. Comparison of the deviation of the 12-month moving average temperature from the temperature mean for the 30-year climate period between 1961 and 1990 for Sutton Bonington.

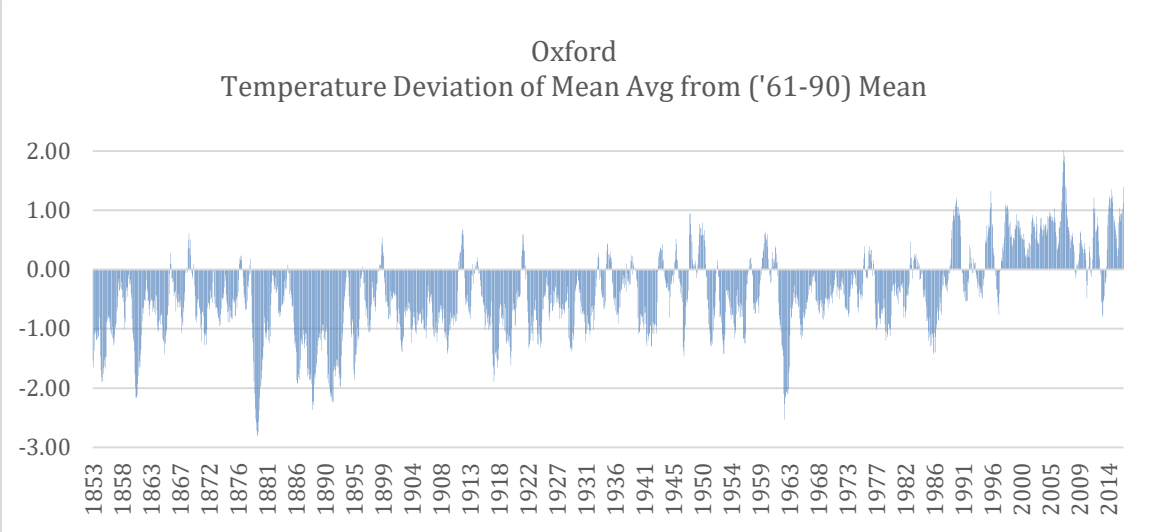

Figure 41. Oxford Temperatures. Comparison of the deviation of the 12-month moving average temperature from the temperature mean for the 30-year climate period between 1961 and 1990 for Oxford.

Central England Precipitation Record (HadUKP). Figure 42 shows the average deviation from the 1961-1990 mean of the annual average Central England Precipitation (Figure 36). Fluctuations are minimal and indicative of the maritime climate.

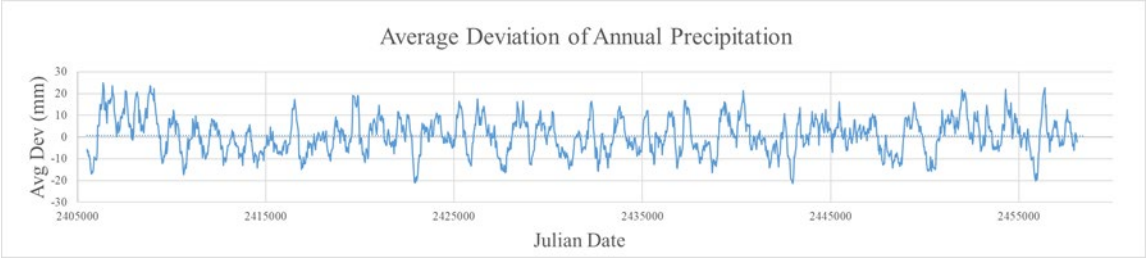

Figure 42. Central England Precipitation - HadUKP

Carbon and Oxygen Isotopes

Isotopic Equilibrium. The formation of calcite in the Netherton Tunnel was determined to be in isotopic equilibrium. Using the Kim and O'Neil equation [9] to derive the fractionation factor (α) for the warm and cold season, the α for the measured temperature in July of 16 °C is 1.03 and represents the warm season. The estimated α value

for the cold season at 8 °C is 1.032. The α for each season was applied to estimate a range -5.90 to -6.23‰ for the $\delta^{18}O$ of the calcite formed. The actual speleothem sample $\delta^{18}O$ values range from -4.2 to -7.2 ‰. The values are very similar and thus, the sampled speleothem can be considered to have formed in isotopic equilibrium.

Speleothem Isotope Record. Figures 43 and 45 are time series of $\delta^{13}C$ and $\delta^{18}O$ values for the speleothem samples N5 and NAC. The age model applied to Sample NAC dates the oldest calcite layer to 1928, to the date of collection, 2016. Annual layering, upon which the age model is based, ranges from 0.2 to 0.8 mm and the drill bit used for sampling had a diameter of 0.5 mm. Sampling, therefore, only has a resolution of 1-2 years at best. Since it is difficult to evaluate the angle of the sampling drill hole, it is reasonable to assume that temporal resolution is generally no better than 3 years of speleothem growth. Therefore, the data are smoothed by a 3-year running average (Figures 44 and 46).

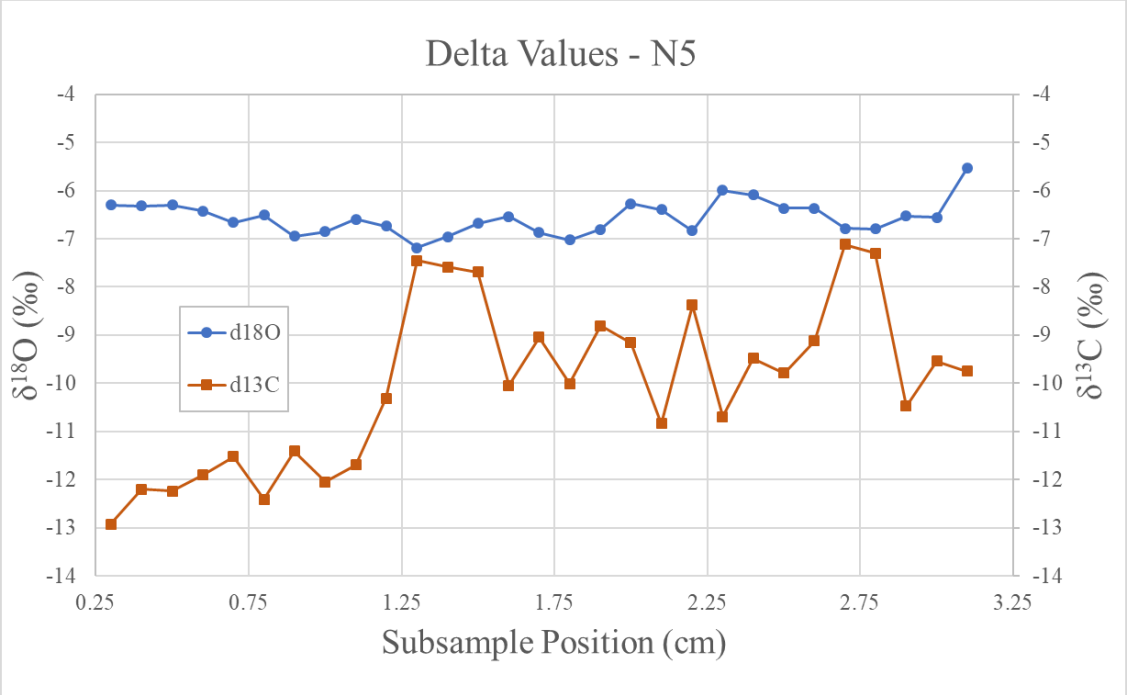

Figure 43. Speleothem Sample N5 Delta Values. There is no age model available for the N5 sample, so the timing of the two δ13C peaks is unknown.

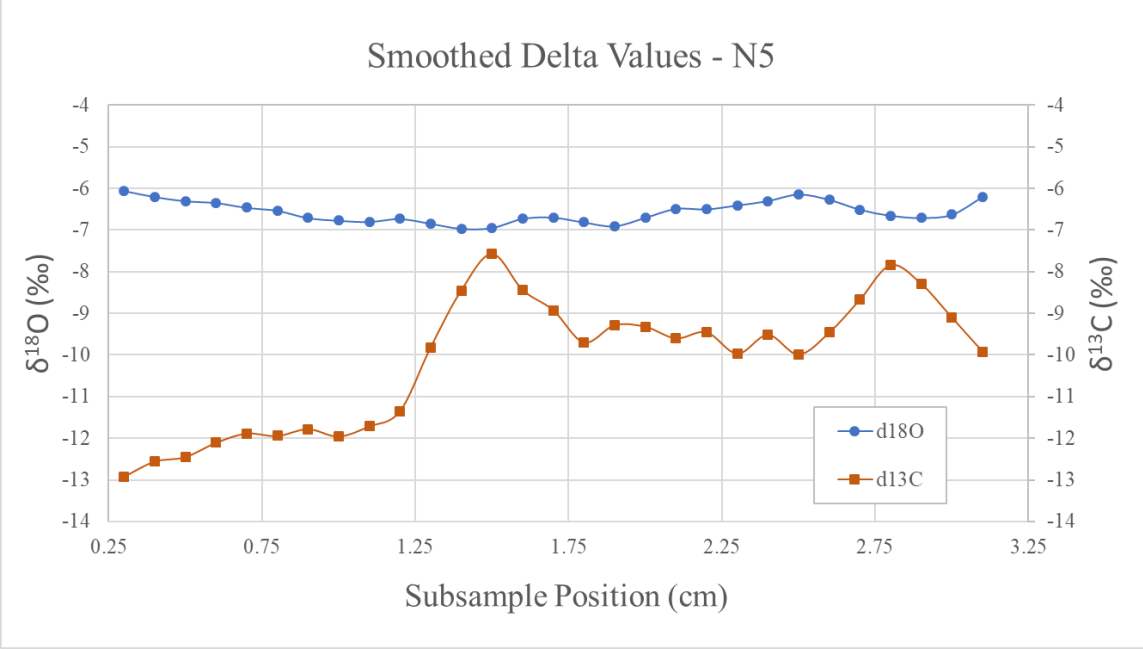

Figure 44. Smoothed Delta Values - Sample N5. (3-point average). There is no age model available for the N5 sample, so the timing of the two $\delta^{13}C$ peaks is unknown.

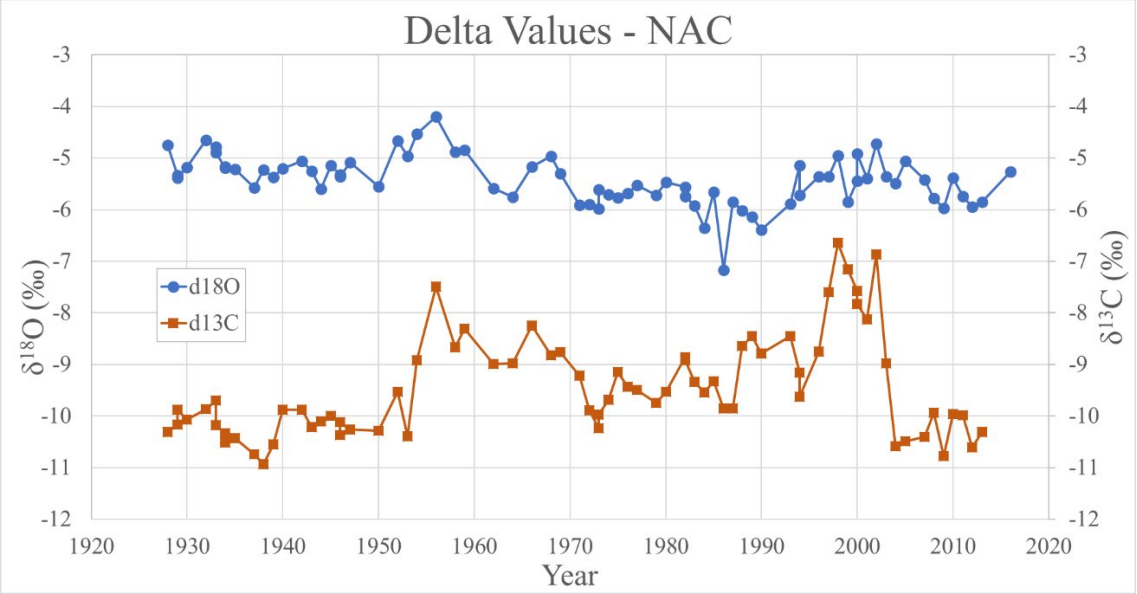

Figure 45. Speleothem Sample NAC Delta Values

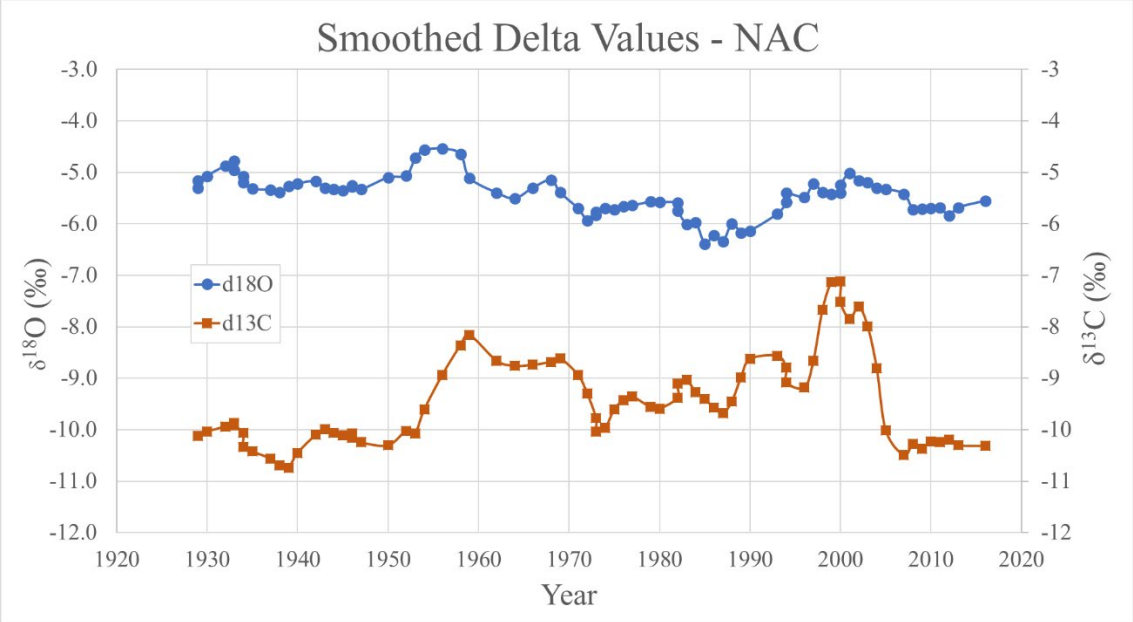

Figure 46. Smoothed Delta Values – Sample NAC. (3-point average)

Land Use

Current Land Use. The area above the tunnels that could conceivably contribute to infiltration is relatively small. Therefore, land use has been relatively consistent above the tunnel (Figure 47). Current land use at Netherton and Wast Hills Tunnels is just over 50% residential and slightly less than 50% pasture, or green space. The area above the Shortwood Tunnel has never been developed and is green space. The overall region is relatively flat with only a few areas of moderate incline interrupting the otherwise flat or gradual inclines of the gently rolling landscape.

Land Use Change. Land use over the Netherton Tunnel changed from rural agricultural at the beginning of the 20th century and is currently residential and green space. The decrease in farming occurring between WWI and WWII was coincident with the migration of the rural population to residential neighborhoods supporting the expansion of industry during this time (Allen, 1929; Nevile et al., 1933). No current industrial areas are active in the immediate study area.

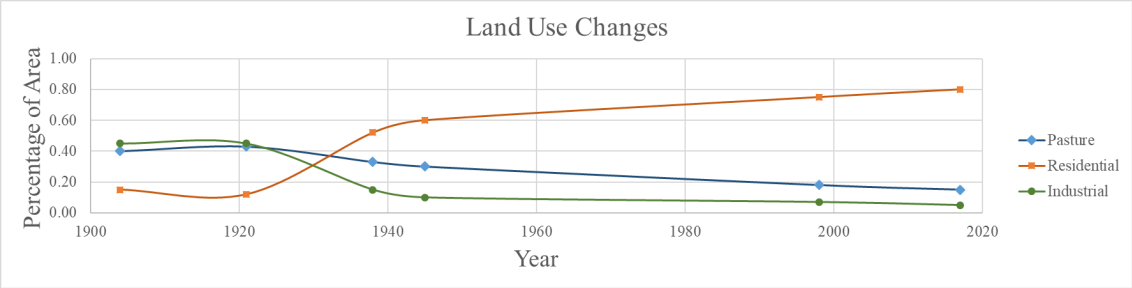

Figure 47. Land Use Change over Netherton Tunnel

Correlation Analyses

A summary of the correlation matrix of all variables with $\delta^{18}O$ and $\delta^{13}C$ is located in Appendix A and graphed in Figure 48. For $\delta^{18}O$, the most significant correlations (Figure

48b) are with multiple-year moving averages of the AMO during the cold season (November through April) and with land use (Figures 48-50). Results of linear regression analysis of $\delta^{18}O$ and the AMO cold season 8-year moving average are tabulated in Table 2. Note the *p-value* of 3.02×10^{-7}, which allows us to reject the null hypothesis that there is no effect of the AMO on speleothem $\delta^{18}O$.

Land use is essentially a categorical variable representing the proportion of residential vs. agricultural areas. Since this is a binary variable (residential or agricultural) the value is expressed as the percentage of residential land use ranging from 0.15 to a maximum of 0.7 (Tables 3 and 4). $\delta^{18}O$ declined as the proportion of residential area land use increased over the past century (p-value < 0.001). The results of single factor Analysis of Variance (ANOVA) allow us to reject the hypothesis that there is no difference in speleothem isotopes between the categorical changes in land use (Table 3).

Similarly, $\delta^{13}C$ increased as the proportion of residential area increased over this time period (p-value < 0.001) (Figures 48, Table 4). There is no correlation between $\delta^{13}C$ and any climate variables, and in general, $\delta^{13}C$ is not correlated with climate.

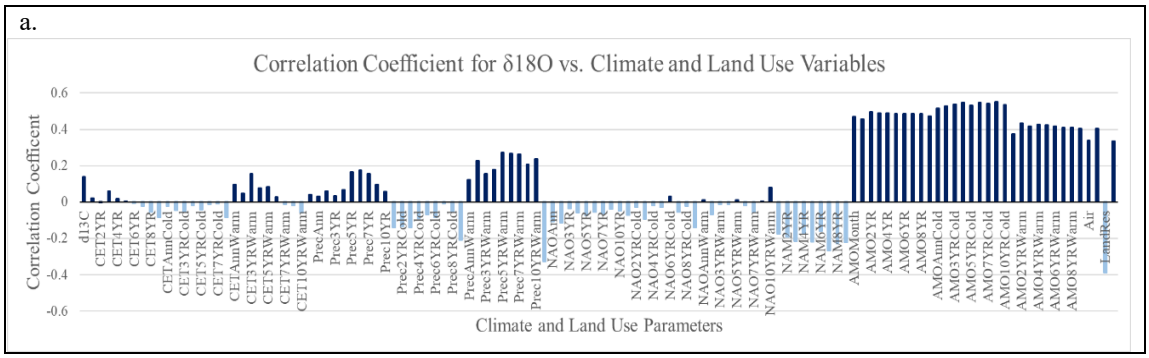

Figure 48. Graphs of Correlation Matrix for $\delta^{13}C$ and $\delta^{18}O$. SAS results between 0.3 and 0.5 indicate a medium/moderate correlation and results greater than 0.5, a large/strong correlation (Kent State University Libraries website). a. Correlation between $\delta^{18}O$ and all climate and land use variables. b. Parameters with significant correlation with $\delta^{18}O$. c. Parameters with significant correlation with $\delta^{13}C$. d. Correlation between $\delta^{13}C$ and all climate and land use variables.

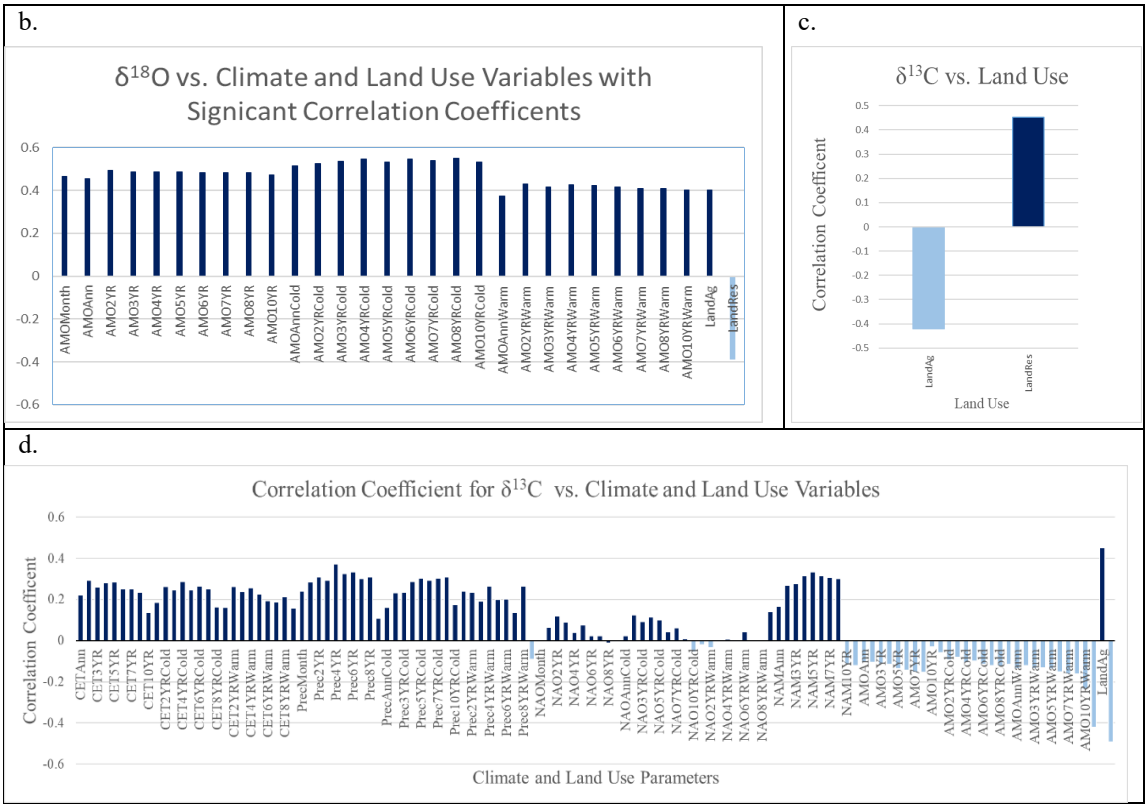

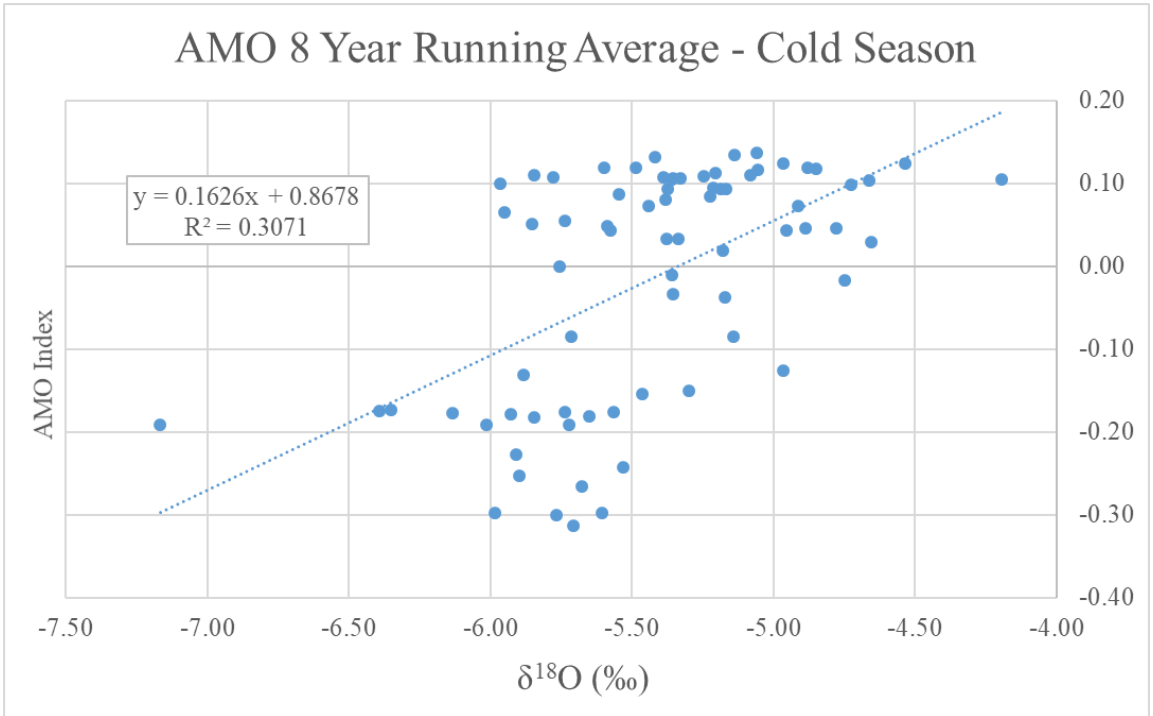

Figure 49. Correlation between Speleothem $\delta^{18}O$ and AMO (p-value < 0.001).

Table 2. Linear Regression Output for AMO and $\delta^{18}O$

SUMMARY OUTPUT		H0:	there is no correlation between 18O and AMO					
		Ha:	there is a correlationm between 18O and AMO					
Regression Statistics								
Multiple R	0.554							
R Square	0.307							
Adjusted R Square	0.297							
Standard Error	0.118							
Observations	74							
ANOVA								
	df	*SS*	*MS*	*F*	*Significance F*			
Regression	1	0.44	0.44	31.91	3.02E-07			
Residual	72	1.00	0.01					
Total	73	1.44						
	Coefficients	*Standard Error*	*t Stat*	*P-value*	*Lower 95%*	*Upper 95%*	*Lower 95.0%*	*Upper 95.0%*
Intercept	0.868	0.157	5.531	0.000	0.555	1.181	0.555	1.181
d18O	0.163	0.029	5.649	0.000	0.105	0.220	0.105	0.220

Figure 50. AMO Index and Speleothem $\delta^{18}O$.

Table 3. ANOVA: Single Factor $\delta^{18}O$ and Land Use

Anova: Single Factor δ18O and Land Use

SUMMARY

Groups	*Count*	*Sum*	*Average*	*Variance*
Land Use Ratio 1	21	-108.7060797	-5.17648	0.061436
Land Use Ratio 2	7	-33.63230595	-4.80462	0.174897
Land Use Ratio 3	31	-177.2214094	-5.71682	0.194132
Land Use Ratio 4	16	-87.55328662	-5.47208	0.135737

ANOVA

Source of Variation	*SS*	*df*	*MS*	*F*	*P-value*	*F crit*
Between Groups	6.665777	3	2.221926	15.56073	7.07E-08	2.733647
Within Groups	10.13813	71	0.142791			
Total	16.80391	74				

Table 4. ANOVA: Single Factor $\delta^{13}C$ and Land Use

Anova: Single Factor δ13C and Land Use

SUMMARY

Groups	*Count*	*Sum*	*Average*	*Variance*
Land Use Ratio 1	21	-214.442	-10.2115	0.094928
Land Use Ratio 2	7	-63.5875	-9.08393	1.115234
Land Use Ratio 3	31	-281.931	-9.09456	0.540472
Land Use Ratio 4	16	-149.599	-9.34997	1.87616

ANOVA

Source of Variation	*SS*	*df*	*MS*	*F*	*P-value*	*F crit*
Between Groups	17.18449	3	5.728164	7.681329	0.000162	2.733647
Within Groups	52.94652	71	0.745726			
Total	70.13101	74				

Discussion

There continues to be a significant interest in climate studies. Reconstruction of past climates, and determining triggers and lag effects of current climate phenomenon, are important for creating records and understanding teleconnections at inter-hemispheric, as well as latitudinal scales. Speleothems can provide an accurate constraint on the timing of climate events compared to other proxies, as well as insight into climate forcings and feedback mechanisms. Speleothems from the tunnels of the canal system in Central

England appeared to experience a rapid growth rate, which is required to detect short-term climate events and low-amplitude climate signals. Additionally, formation in an artificial structure of a known age constrains the period of a potential record. This might be the only study that would document recent climate change in Great Britain.

This study seeks to determine whether tunnel speleothems act as reliable climate proxies. Speleothems in this study are growing at a rate of 0.4 -1.0 mm per year, a deposition rate that could provide a high-resolution environmental record of climate and land use. Calcite layers form in isotopic equilibrium via infiltration of precipitation from the surface that has a residence time of less than a year, and thus is likely to record annual changes.

Our age model based on annual layering, is used as an alternative to radiometric dating methods. The age model applied to Sample NAC from the Netherton tunnel is based primarily on confocal microscopy and fluorescence of organics, mineralogical characteristics, and Sr/Ca ratio. All three of these indices provide nearly identical ages, therefore the age model seems reasonable given the time of construction of the tunnel (1858) and the sampling depth.

Subsampling with a 0.5mm dental drill bit at regular intervals resulted in a time series of isotope values averaged over approximately 3-4 layers with a bias against thinner layers (Quinn et al., 1996; McDermott, 2004; Baldini et al., 2008). In order to compare these isotope values to climate records, averages of shorter-term climate data were required.

Figure 46 shows temporal variation of $\delta^{13}C$ of 2 - 4‰. Although there is no strong correlation with environmental variables, there appears to be a correlation with land use changes (Figure 47, Table 4), even though land use is a categorical variable that is difficult to interpret. Agriculture in the early 20th century transitioned to residential and green space by about 1940. Without knowledge of the type of row crops that were grown and the vegetation history after about 1940, correlation with $\delta^{13}C$ is difficult. Increased infiltration of meteoric water associated with farmland possibly increases the flow of percolating water, therefore limiting the extent of interaction in the bedrock compared to residential areas.

The anomalous ^{14}C analyses indicate very low values of percent modern carbon (20 pMC). The non-hyperalkaline conditions and low modern carbon content suggest free exchange of DIC with ancient or "dead" carbon in the bedrock (Tanahara, 1998; Gascoyne and Nelson, 1983; I. Fairchild, personal communication, March 2, 2019). Biotic respiration in geologically ancient bedrock could also mask modern atmospheric ^{14}C (Kilin, 2000). Particulate organic carbon contamination from diesel engines and coal-burning heating systems is also a possible explanation for the low percent modern carbon determined by ^{14}C analyses.

The only strong correlation of $\delta^{18}O$ is with the climate teleconnection influences of the AMO and land use. Shifts from negative to positive AMO are related to shifts in cold to warm periods in the Northern Hemisphere (Zampieri et al., 2017). Positive shifts in $\delta^{18}O$ values, which also indicate warming phases, correlate to these positive shifts in AMO (Figure 49).

Agricultural and industrial land use changes are positively correlated with $\delta^{18}O$ while residential land use changes correlate negatively. This is interpreted as a result of higher infiltration rates associated with agricultural land use compared to residential land use, which allows for more communication, even during the warm season with the effect of evapotranspiration associated with crops, between the atmospheric and the tunnel environments. When residential land use became more prevalent, the $\delta^{18}O$ values decreased. The inverse relationship between $\delta^{18}O$ and residential land use is likely attributed to greater infiltration during the cold season when the mix of lawn and parkland vegetation is dormant, leading to a larger influence of the colder season on isotope values of the water percolating through the bedrock to the tunnel.

The Sr/Ca of the speleothem demonstrates seasonal variations in the trace element indicating annual layering. Differences in the seasonal fluctuation of rainfall is often responsible but in the UK's maritime climate the annual variations in Sr/Ca are likely the result of evapotranspiration and not related to seasonal rainfall. During the full vegetative state of the warm season, little or no meteoric water infiltrates through the soil zone because of vegetative uptake. This demand on the meteoric water synthesizes relatively dry conditions for the various carbonate phase transitions and speleothem development. In this setting, it is likely Sr is sequestered during the warm season. Strontium composition can also respond to changes in land cover and use, over decades as well as seasonally.

A LWML was created from isotopic analysis of local meteoric water. Figure 26 graphs LMWL along with the isotope values of tunnel drip and puddle water, and describes the isotopic transition of the water at each stage as it migrates from the surface to the

puddles. For each stage, the slope of the trendline signifies the extent of evaporative processes, and the y intercept, which represents deuterium excess (d), results from relative humidity and moisture recycling. The slope and d for each stage progressively decrease, indicating increased evaporation and less moisture recycling at each junction.

The ^{18}O isotope signals do not appear to reflect the long-term climate-warming trend seen in the CET, likely because warming temperature trends have surfaced only in the most recent few decades at a rate of one degree Celsius per 30 years. It is also possible detailed climate information was not recorded in the tunnel speleothem because the climate change is not large enough to overwhelm the variability caused by local environmental inputs. Successfully retrieved, high-resolution records from cave speleothems are located in regions that have highly contrasting seasons (Johnson et al., 2006; Burns et al., 2002; McDermott, 2004). Other successful records derive from speleothems that have formed over tens of thousands of years, during which timeframe climate variation is more substantial (Brook, et al.,2006; Barr-Matthews et al., 1998; McDermott, 2004). Additionally, alternative methods might improve interpretation of speleothem isotope records. Laser ablation or micro-milling subsampling, and exploring new laboratory options for radiometric U-Th dating would increase the resolution of the isotope data (McDermott, 2004). A finer analytical process using the combination of MAT and tunnel temperature might account for variations in the $\delta^{18}O$ from tunnel temperature, and define the impact of MAT alone on $\delta^{18}O$ along shorter time scales.

Conclusions

The results of this investigation indicate that the time series of $\delta^{18}O$ in tunnel speleothems exhibit moderate, statistically-significant correlation with the AMO index, which is a measure of variations of sea-surface temperature anomalies on multi-decadal time scales. In addition, correlation of $\delta^{18}O$ and $\delta^{13}C$ with residential land-use is consistent with infiltration biased toward the winter season. $\delta^{18}O$ is negatively correlated with land use; as the percentage of residential land use increases, $\delta^{18}O$ becomes slightly more negative. Residential/greenspace areas have reduced infiltration during the growing season as vegetation sequesters and transpires most of the available water. Infiltration rates are higher during the cold season when vegetation is dormant. $\delta^{13}C$ is positively correlated with residential land use. The reason for this trend is not clear; however, if most of the infiltration occurs during the cold months, then soil microbial activity would be at a minimum.

It is unclear whether a record of shorter-term local environmental signals is retrievable from these or similar speleothems. In this study, we suggest that local environmental signals, if present, are likely lost in variability of the maritime climate and geochemical processes in the soil and vadose zone. This may not, however, be the general case for all similar speleothems.

The correlation of $\delta^{18}O$ in tunnel speleothems and the AMO index could be of interest on a larger scale. Over the past couple of decades, increasing hurricane frequency and increased melting of the Greenland Ice Sheet have been attributed to warming sea-surface temperatures over the North Atlantic (Ting et al., 2009). Whether this increase in

SST in related to human-induced, long-term climate change or natural variability in the AMO is a topic of debate (*e.g.* Emanuel, 2005; Webster et al., 2005; Landsea, 2005). The climate data preserved in the tunnel speleothems could be of value in climate modeling with the current focus on teleconnections. In addition, the record of land use changes from tunnel speleothems has the potential to assist in monitoring changes in land cover and the impact of anthropogenic activities on area hydrology.

The AMO index describes the multi-decadal climate variability in North Atlantic by spatially averaging SST anomalies. A future approach, suggested by Dr. Byron Steinman (personal communication, 2019), would entail analysis of individual grid cells of instrument data and comparing North Atlantic SST of specific regions to the spatial time series to the $\delta^{18}O$ time series of the tunnel speleothems. The process may identify regions of the North Atlantic where sea surface temperatures are better correlated with the $\delta^{18}O$ record.

Analysis of speleothems from the tunnels on the BCN that are the focus of this investigation suggest that high-resolution paleoenvironmental records can be obtained from similar deposits found in other constructed features.

References

Air mass types. (n.d.). Retrieved from https://www.metoffice.gov.uk/weather/learn-about/weather/atmosphere/air-masses/types

Affek, H., & Yakir, D. (2014). The Stable Isotopic Composition of Atmospheric CO2. *Treatise on Geochemistry,*179-212. doi:10.1016/b978-0-08-095975-7.00407-1

Akers, P. D., Brook, G. A., Railsback, L. B., Liang, F., Iannone, G., Webster, J. W., . . . Edwards, R. L. (2016). An extended and higher-resolution record of climate and land use from stalagmite MC01 from Macal Chasm, Belize, revealing connections between major dry events, overall climate variability, and Maya sociopolitical changes. Palaeogeography, Palaeoclimatology, Palaeoecology, 459, 268-288. doi:10.1016/j.palaeo.2016.07.007

Alexander, L.V. and Jones, P.D. (2001). Updated precipitation series for the U.K. and discussion of recent extremes, *Atmospheric Science Letters*. doi:10.1006/asle.2001.0025

Allen, C.C. (1929). The Industrial Development of Birmingham and the Black Country 1960-1927. Franc Cass and Co. Ltd.

Ambaum, M. H., B. J. Hoskins, and D. B. Stephenson. (2001). Arctic Oscillation or North Atlantic Oscillation? *J. Climate*, *14*, 3495–3507. doi.org/10.1175/1520-0442(2001)014<3495:AOONAO>2.0

Andrews, J. A., & Schlesinger, W. H. (2001). Soil CO_2 dynamics, acidification, and chemical weathering in a temperate forest with experimental CO_2

enrichment. *Global Biogeochemical Cycles,15*(1), 149-162. doi:10.1029/2000gb001278

Atkinson, T. C., Harmon, R. S., Smart, P. L., & Waltham, A. C. (1978). Palaeoclimatic and geomorphic implications of 230Th/234U dates on speleothems from Britain. Nature, 272(5648), 24-28. doi:10.1038/272024a0

Aviation, G. (2015, November). Global climate in context as the world approaches 1°C above pre-industrial for the first time. Retrieved January 25, 2016, from https://www.metoffice.gov.uk/research/news/2015/global-average-temperature-2015

Baldini, J., Mcdermott, F., & Fairchild, I. (2006). Spatial variability in cave drip water hydrochemistry: Implications for stalagmite paleoclimate records. Chemical Geology, 235(3-4), 390-404. doi:10.1016/j.chemgeo.2006.08.005

Baker, A., Ito, E., Smart, P. L., & Mcewan, R. F. (1997). Elevated and variable values of ^{13}C in speleothems in a British cave system. Chemical Geology, 136(3-4), 263-270. doi:10.1016/s0009-2541(96)00129-5

Baker, A., Smart, P. L., & Edwards, R. L. (1995). Paleoclimate implications of mass spectrometric dating of a British flowstone. *Geology,23*(4), 309. doi:10.1130/0091-7613(1995)0232.3.co;2

Bar-Matthews, M., Ayalon, A., & Kaufman, A. (1998). Middle to Late Holocene (6,500 Yr. Period) Paleoclimate in the Eastern Mediterranean Region from Stable Isotopic Composition of Speleothems from Soreq Cave, Israel. Water Science and

Technology Library Water, Environment and Society in Times of Climatic Change, 203-214. doi:10.1007/978-94-017-3659-6_9

Benner, T. C. (1999). Central England temperatures: Long-term variability and teleconnections. *International Journal of Climatology,19*(4), 391-403. doi:10.1002/(sici)1097-0088(19990330)19:43.0.co;2-z

Besly, B. M., & Cleal, C. J. (1997). Upper Carboniferous stratigraphy of the West Midlands (UK) revised in the light of borehole geophysical logs and detrital compositional suites. *Geological Journal,32*(2), 85-118. doi:10.1002/(sici)1099-1034(199706)32:23.3.co;2-f

Besly, B. M., & Turner, P. (1983). Origin of red beds in a moist tropical climate (Etruria Formation, Upper Carboniferous, UK). *Geological Society, London, Special Publications,11*(1), 131-147. doi:10.1144/gsl.sp.1983.011.01.14

Blyth, A. J., Hartland, A., & Baker, A. (2016). Organic proxies in speleothems – New developments, advantages and limitations. *Quaternary Science Reviews,149*, 1-17. doi:10.1016/j.quascirev.2016.07.001

Blyth, A. J., Hua, Q., Smith, A., Frisia, S., Borsato, A., & Hellstrom, J. (2017). Exploring the dating of "dirty" speleothems and cave sinters using radiocarbon dating of preserved organic matter. *Quaternary Geochronology,39*, 92-98. doi:10.1016/j.quageo.2017.02.002

Brook, G. A., Ellwood, B. B., Railsback, L. B., & Cowart, J. B. (2006). A 164 ka record of environmental change in the American Southwest from a Carlsbad Cavern

speleothem. Palaeogeography, Palaeoclimatology, Palaeoecology, 237(2-4), 483-507. doi:10.1016/j.palaeo.2006.01.001

Burns, S. J. (2002). A 780-year annually resolved record of Indian Ocean monsoon precipitation from a speleothem from south Oman. *Journal of Geophysical Research,107*(D20). doi:10.1029/2001jd001281

Can, A., and A. T. Atimtay. (2002). Time series analysis of mean temperature data in Turkey. *Applied Time Series*, *4*, 20–23.

Cerling, T. E., Solomon, D., Quade, J., & Bowman, J. R. (1991). On the isotopic composition of carbon in soil carbon dioxide. *Geochimica Et Cosmochimica Acta,55*(11), 3403-3405. doi:10.1016/0016-7037(91)90498-t

Clark, I. D., & Fritz, P. (1999). *Environmental isotopes in hydrogeology*. Boca Raton: Lewis Publ.

Cotton, P.A. (2003). Avian migration phenology and global climate change, *Proceedings of the National Academy of Sciences*,*100*(21), 12212-12222. doi.org/10.1073/pnas.1930548100

Craig, H., Gordon, L. (1965). Deuterium and oxygen-18 variations in the ocean and marine atmosphere, *Stable Isotopes in Oceanographic Studies and Paleo-Temperatures*, ed. E Tongiorgi, 9-130.

Cragg, R. (1997). *Wales and West Central England*. London: Telford.

Cumberlidge, J. (2009). *Inland Waterways of Great Britain*. Imray,Laurie,Norie & Wilson Lt. 339.

Cunningham, W.P, Cunningham, M.A.(2011). *Environmental Science: a Global Concern*. *11th ed.,* McGraw-Hill Education, 321.

Dansgaard, W. (1964). Stable isotopes in precipitation. Tellus, 16(4), 436-468. doi:10.3402/tellusa.v16i4.8993

Dorale, J. A., Edwards, R. L., Alexander, E. C., Shen, C., Richards, D. A., & Cheng, H. (2004). Uranium-Series Dating of Speleothems: Current Techniques, Limits, & Applications. *Studies of Cave Sediments,*177-197. doi:10.1007/978-1-4419-9118-8_10

Dreybrodt, W. (2008). "Evolution of the isotopic composition of carbon and oxygen in a calcite precipitating $H_2O–CO_2–CaCO_3$ solution and the related isotopic composition of calcite in stalagmites," Geochimica Cosmochimica Acta 72, 4712–4724. Geochimica Et Cosmochimica Acta, 72(24), 6198. doi:10.1016/j.gca.2008.10.008

Duplessy, J. C., Labeyrie, J., Lalou, C., & Nguyen, H. V. (1970). Continental Climatic Variations between 130,000 and 90,000 Years BP. Nature, 226(5246), 631-633. doi:10.1038/226631a0

Emanuel, K. (2005). Increasing destructiveness of tropical cyclones over the past 30 years. Nature, 436(7051), 686.

Epstein, S., Buchsbaum, R., Lowenstam, H. A., & Urey, H. C. (1953). Revised Carbonate-Water Isotopic Temperature Scale. Geological Society of America Bulletin, 64(11), 1315. doi:10.1130/0016-7606(1953)64[1315:rcits]2.0.co;2

Fairchild, I. J., Borsato, A., Tooth, A. F., Frisia, S., Hawkesworth, C. J., Huang, Y., . . . Spiro, B. (2000). Controls on trace element (Sr–Mg) compositions of carbonate cave waters: Implications for speleothem climatic records. *Chemical Geology,166*(3-4), 255-269. doi:10.1016/s0009-2541(99)00216-8

Fairchild, I. J., Smith, C. L., Baker, A., Fuller, L., Spötl, C., Mattey, D., . . . E.i.m.f. (2006). Modification and preservation of environmental signals in speleothems. Earth-Science Reviews, 75(1-4), 105-153. doi:10.1016/j.earscirev.2005.08.003

Farquhar, G.D., Ehleringer, J.R., Hubick, K.T.(1989). Carbon Isotope Discrimination and Photosynthesis. *Annual Review of Plant Physiology and Plant Molecular Biology,40*(1), 503-537. doi:10.1146/annurev.arplant.40.1.503

Fitter, A. H., Fitter, R.S.R. (2002). Rapid Changes in Flowering Time in British Plants. *Science, 296*(5573), 1689-1691. doi:10.1126/science.1071617

Gascoyne, M. (1992). Palaeoclimate determination from cave calcite deposits. *Quaternary Science Reviews, 11*(6), 609-632. doi:10.1016/0277-3791(92)90074-i

Gascoyne, M., & Nelson, D. E. (1983). Growth Mechanisms of Recent Speleothems from Castleguard Cave, Columbia Icefields, Alberta, Canada, Inferred from a Comparison of Uranium-Series and Carbon-14 Age Data. Arctic and Alpine Research, 15(4), 537. doi: 10.2307/1551239

Gat, J. R. (1971). Comments on the Stable Isotope Method in Regional Groundwater Investigations. Water Resources Research, 7(4), 980–993. doi: 10.1029/wr007i004p00980

Gat, J. R. (1971). Comments on the Stable Isotope Method in Regional Groundwater Investigations. Water Resources Research, 7(4), 980–993. doi: 10.1029/wr007i004p00980

"Geology of the West Midlands Branch Area." *Vesuvius: The Most Dangerous Volcano in the World?*, 7 July 2011, ougs.org/westmidlands/local-geology/.

Hadley Centre for Climate Prediction and Research (2006): Met Office Hadley Centre Central England Temperature (HadCET) Series. NCAS British Atmospheric Data Centre. Retrieved from https://catalogue.ceda.ac.uk/uuid/a946415f9345f6da9bf4c475c19477b6

Hendy, C. (1971). The isotopic geochemistry of speleothems—I. The calculation of the effects of different modes of formation on the isotopic composition of speleothems and their applicability as palaeoclimatic indicators. Geochimica Et Cosmochimica Acta,35(8), 801-824. doi:10.1016/0016-7037(71)90127-x

Hodge, E., Mcdonald, J., Fischer, M., Redwood, D., Hua, Q., Levchenko, V., . . . Fink, D. (2011). Using the 14C Bomb Pulse to Date Young Speleothems. *Radiocarbon,53*(2), 345-357. doi:10.1017/s0033822200056605

Huang, Y., Fairchild, I. J., Borsato, A., Frisia, S., Cassidy, N. J., Mcdermott, F., & Hawkesworth, C. J. (2001). Seasonal variations in Sr, Mg and P in modern speleothems (Grotta di Ernesto, Italy). *Chemical Geology,175*(3-4), 429-448. doi:10.1016/s0009-2541(00)00337-5

Hurrell, J. W., Kushnir, Y., Ottersen, G., & Visbeck, M. (2003). An overview of the North Atlantic Oscillation. *The North Atlantic Oscillation: Climatic Significance*

*and Environmental Impact Geophysical Monograph Series,*1-35. doi:10.1029/134gm01

Hurrell, J. W. (2003). *The North Atlantic oscillation: Climatic significance and environmental impact*. Washington, DC: American Geophysical Union. ISBN 9780875909943.

Hurrell, James & National Center for Atmospheric Research Staff (Eds). Last modified 04 Aug 2018. "The Climate Data Guide: Hurrell North Atlantic Oscillation (NAO) Index (station-based)." Retrieved from https://climatedataguide.ucar.edu/climate-data/hurrell-north-atlantic-oscillation-nao-index-station-based.

Inkpen, R. R. (2013). Reconstructing past atmospheric pollution levels using gravestone erosion rates. *Area,45*(3), 321-329. doi:10.1111/area.12035

Jenkins, G, Perry, M and Prior, J. (2008). The climate of the United Kingdom and recent trends. Met Office Hadley Center, Exeter, UK. *UK Climate Projections*, *4*, 119. ISBN 978-1-906360-05-4. Retrieved 2018 from http://www.homepages.ed.ac.uk/shs/Climatechange/Data%20sources/UKCIPTrends.pdf

Jex, C. N., Baker, A., Fairchild, I. J., Eastwood, W. J., Leng, M. J., Sloane, H. J., . . . Bekaroğlu, E. (2010). Calibration of speleothem $\delta^{18}O$ with instrumental climate records from Turkey. Global and Planetary Change, 71(3-4), 207-217. doi:10.1016/j.gloplacha.2009.08.004

Johnson, K., Hu, C., Belshaw, N., & Henderson, G. (2006). Seasonal trace-element and stable-isotope variations in a Chinese speleothem: The potential for high-resolution paleomonsoon reconstruction. *Earth and Planetary Science Letters,244*(1-2), 394-407. doi:10.1016/j.epsl.2006.01.064

Jones, P. D., Jonsson, T., & Wheeler, D. (2018, January 2). Climatic Research Unit: Data: North Atlantic Oscillation (NAO). Retrieved April, 2019, from https://crudata.uea.ac.uk/cru/data/nao/nao.dat

Jones, P. D., Jonsson, T., & Wheeler, D. (1997). Extension to the North Atlantic oscillation using early instrumental pressure observations from Gibraltar and south-west Iceland. *International Journal of Climatology,17*(13), 1433-1450. doi:10.1002/(sici)1097-0088(19971115)17:133.0.co;2-p

Kashiwaya, K., Atkinson, T. C., & Smart, P. L. (1991). Periodic Variations in Late Pleistocene Speleothem Abundance in Britain. *Quaternary Research, 35*(2), 190-196. doi:10.1016/0033-5894(91)90066-e

Kauserud, H., Heegaard, E., Buntgen, U., Halvorsen, R., Egli, S., Senn-Irlet, B., . . . Stenseth, N. C. (2012). Warming-induced shift in European mushroom fruiting phenology. *Proceedings of the National Academy of Sciences,109*(36), 14488-14493. doi:10.1073/pnas.1200789109

Keeling, C. D. (1979). The Suess effect: 13Carbon-14Carbon interrelations. *Environment International,2*(4-6), 229-300. doi:10.1016/0160-4120(79)90005-9

Kendall, C., & McDonnell, J. J. (2006). *Isotope tracers in catchment hydrology*. Amsterdam: Elsevier.

Kendon, M., McCarthy, M., Jevrejeva, S. and Legg, T. (2017) State of the UK Climate 2016. UK: Met Office Exeter.

Lachniet, M.S. (2009). Climatic and environmental controls on speleothem oxygen-isotope values. *Quaternary Science Reviews,28*, 412–432.

Landsea, C. W. (2005). Meteorology: hurricanes and global warming. Nature, 438(7071), E11.

Long, A. & Putnam, L.(2004). Linear model describing three components of flow in karst aquifers using ^{18}O data. Journal of Hydrology. doi:10.1016/s0022-1694(04)00190-8

Manley, G. (1977). Annual rainfall in England since 1725: Some comments. Quarterly Journal of the Royal Meteorological Society, 103(438), 820-823. doi:10.1002/qj.49710343824

Menzel, A., & Fabian, P. (1999). Growing season extended in Europe. *Nature,397*(6721), 659-659. doi:10.1038/17709

Mattey, D., Lowry, D., Duffet, J., Fisher, R., Hodge, E., & Frisia, S. (2008). A 53 year seasonally resolved oxygen and carbon isotope record from a modern Gibraltar speleothem: Reconstructed drip water and relationship to local precipitation. *Earth and Planetary Science Letters,269*(1-2), 80-95. doi:10.1016/j.epsl.2008.01.051

Mayes, J., & Wheeler, D. (2013). Regional weather and climates of the British Isles - Part 1: Introduction. *Weather,68*(1), 3-8. doi:10.1002/wea.2041

Mccrea, J. M. (1950). On the Isotopic Chemistry of Carbonates and a Paleotemperature Scale. *The Journal of Chemical Physics,18*(6), 849-857. doi:10.1063/1.1747785

Mcdermott, F. (2004). Palaeo-climate reconstruction from stable isotope variations in speleothems: A review. *Quaternary Science Reviews,23*(7-8), 901-918. doi:10.1016/j.quascirev.2003.06.021

Mooers, H. D., Loeffler, S., Myrbo, A. (2014, October 22). "Historical Record of Industrial Pollution Recovered from Abandoned Canals, Black Country, West Midlands, UK," GSA Annual Meeting in Vancouver, British Columbia Paper 295-11 Session No. 295, Booth #23

Mooers, H., Carlson, M., Harrison, R., Inkpen, R., & Loeffler, S. (2017). Correlation of gravestone decay and air quality 1960–2010. *Atmospheric Environment,152*, 156-171. doi:10.1016/j.atmosenv.2016.12.026

Mooers, H. D., Cota-Guertin, A. R., Regal, R. R., Sames, A. R., Dekan, A. J., & Henkels, L. M. (2016). A 120-year record of the spatial and temporal distribution of gravestone decay and acid deposition. *Atmospheric Environment,127*, 139-154. doi:10.1016/j.atmosenv.2015.12.023

Nevile, G. H., Lymington, V., Orwin, C.S., Brown, A.H., Wolton, E.D., Dudley, R., Greig, R., Keen, B.A., (1933) Discussion [PDF file]. *Mechanization and British Agriculture*. pp 31 – 50.

North Atlantic Oscillation (2019, June). Retrieved from https://www.ncdc.noaa.gov/teleconnections/nao/

The North Atlantic Oscillation: Climatic Significance and Environmental Impact, (2011, June 3). *Eos,84(8),*73-74. Retrieved from https://agupubs.onlinelibrary.wiley.com/doi/pdf/10.1029/2003EO080005

Parker, D. E., Legg, T. P., & Folland, C. K. (1992). A new daily central England temperature series, 1772–1991. *International Journal of Climatology,12*(4), 317-342. doi:10.1002/joc.3370120402

Pfahl, S., & Sodemann, H. (2013). What controls deuterium excess in global precipitation? *Climate of the Past Discussions,9*(4), 4745-4770. doi:10.5194/cpd-9-4745-2013

Plummer, C. C., Carlson, D. H., & Hammersley, L. (2001). *Physical geology*. New York, NY: McGraw-Hill Education. 114.

Proctor, C. J., Baker, A., Barnes, W. L., & Gilmour, M. A. (2000). A thousand year speleothem proxy record of North Atlantic climate from Scotland. *Climate Dynamics,16*(10-11), 815-820. doi:10.1007/s003820000077

Quinn, T. M., Taylor, F. W., Crowley, T. J., & Link, S. M. (1996). Evaluation of sampling resolution in coral stable isotope records: A case study using records from New Caledonia and Tarawa. Paleoceanography, 11(5), 529-542. doi:10.1029/96pa01859

Rodwell, M. J., Rowell, D. P., & Folland, C. K. (1999). Oceanic forcing of the wintertime North Atlantic Oscillation and European climate. *Nature,398*(6725), 320-323. doi:10.1038/18648

Rozanski, K., Araguás-Araguás, L., & Gonfiantini, R. (2013). Isotopic Patterns in Modern Global Precipitation. Climate Change in Continental Isotopic Records Geophysical Monograph Series, 1-36. doi:10.1029/gm078p0001

Schwarcz, H. (1986). Geochronology and Isotopic Geochemistry of Speleothems. The Terrestrial Environment, B, 271-303. doi:10.1016/b978-0-444-42225-5.50012-7

Schwarcz, H. (2007). CARBONATE STABLE ISOTOPES | Speleothems. *Encyclopedia of Quaternary Science,*290-300. DOI: 10.1016/B0-44-452747-8/00352-5

Sharp, T. (2017, October 13). Earth's Atmosphere: Composition, Climate & Weather. Retrieved from https://www.space.com/17683-earth-atmosphere.html

Self, C. A., & Hill, C. A. (2003). How speleothems grow: An introduction to the ontogeny of cave minerals. Journal of Cave and Karst Studies, 65(2), 130-151.

Sharp, Z. (2017). *Principles of Stable Isotope Geochemistry 2nd edition*. Upper Saddle River, NJ: Pearson/Prentice Hall.

Simpson, I. R., & Jones, P. D. (2011). Updated precipitation series for the UK derived from Met Office gridded data. International Journal of Climatology, 32(15), 2271-2282. doi:10.1002/joc.3397

Sparks, T., & Crick, H. (2015). *The impact of climate change on biological phenology in the UK* (pp. 1-31, Tech. No. 12). Natural Environment Research Council. doi:https://nerc.ukri.org/research/partnerships/ride/lwec/report-cards/biodiversity-source12/

Tan, L., Orland, I., & Cheng, H. (2014). Annually laminated speleothems in paleoclimate studies. *Past Global Changes Magazine,22*(1), 22-23. doi:10.22498/pages.22.1.22

Team, E. W. (2005, October 01). ESRL Global Monitoring Division - Education and Outreach. Retrieved from https://www.esrl.noaa.gov/gmd/outreach/isotopes/c13tellsus.html

Thackeray, S. J., Sparks, T. H., Frederiksen, M., Burthe, S., Bacon, P. J., Bell, J. R., . . . Wanless, S. (2010). Trophic level asynchrony in rates of phenological change for marine, freshwater and terrestrial environments. *Global Change Biology,16*(12), 3304-3313. doi:10.1111/j.1365-2486.2010.02165.x

Thompson, D. W. (2001). Regional Climate Impacts of the Northern Hemisphere Annular Mode. *Science,293*(5527), 85-89. doi:10.1126/science.1058958

Ting, M., Kushnir, Y., Seager, R., & Li, C. (2009). Forced and internal twentieth-century SST trends in the North Atlantic. Journal of Climate, 22(6), 1469-1481.

Trenberth, K., & Zhang, R. (2019, January 10). The Climate Data Guide: Atlantic Multi-decadal Oscillation (AMO). Retrieved from https://climatedataguide.ucar.edu/climate-data/atlantic-multi-decadal-oscillation-amo

Webster, P. J., Holland, G. J., Curry, J. A., & Chang, H. R. (2005). Changes in tropical cyclone number, duration, and intensity in a warming environment. Science, 309(5742), 1844-1846.

West Midlands History. (2019). Coal, Iron, Limestone, Clay – Discovering the Foundation of Black Country History. Retrieved July 18,2018 from https://historywm.com/podcasts/coal-iron-limestone-clay-discovering-the-foundation-of-black-country-history.

Wigley, T. M., Lough, J. M., & Jones, P. D. (1984). Spatial patterns of precipitation in England and Wales and a revised, homogeneous England and Wales precipitation series. Journal of Climatology, 4(1), 1-25. doi:10.1002/joc.3370040102

Zampieri, M., Toreti, A., Schindler, A., Scoccimarro, E., & Gualdi, S. (2017). Atlantic multi-decadal oscillation influence on weather regimes over Europe and the Mediterranean in spring and summer. *Global and Planetary Change,151*, 92-100. doi:10.1016/j.gloplacha.2016.08.014

Appendix

Appendix A. Correlation Coefficients for all variables vs. $\delta^{18}O$ and $\delta^{13}C$

Parameter	Correlation with $\delta^{18}O$	Correlation with $\delta^{13}C$
$\delta^{18}O$	1	0.13757
$\delta^{13}C$	0.13757	1
CETAnn	0.02053	0.24514
CET2YR	-0.00039	0.22264
CET3YR	0.06085	0.29419
CET4YR	0.01569	0.2597
CET5YR	0.00117	0.28225
CET6YR	-0.00434	0.2863
CET7YR	-0.02147	0.25107
CET8YR	-0.0563	0.2525
CET10YR	-0.08353	0.23522
CETAnnCold	-0.02152	0.13681
CET2YRCold	-0.04504	0.18478
CET3YRCold	-0.0539	0.26341
CET4YRCold	-0.0196	0.24698
CET5YRCold	-0.04194	0.28723
CET6YRCold	-0.01177	0.2468
CET7YRCold	-0.00967	0.2656
CET8YRCold	-0.08278	0.25264
CETAnnWarm	0.09733	0.16401
CET2YRWarm	0.04581	0.16109
CET3YRWarm	0.15538	0.26227
CET4YRWarm	0.07709	0.2374
CET5YRWarm	0.08431	0.25798
CET6YRWarm	0.02872	0.22742
CET7YRWarm	-0.01175	0.19395
CET8YRWarm	-0.01946	0.19016
CET10YRWarm	-0.05909	0.21384
PrecMonth	0.0396	0.15729
PrecAnn	0.03102	0.24102
Prec2YR	0.05942	0.28574
Prec3YR	0.03213	0.31007
Prec4YR	0.06576	0.29196

Prec5YR	0.16311	0.37418
Prec6YR	0.17411	0.3261
Prec7YR	0.15372	0.33451
Prec8YR	0.0942	0.30107
Prec10YR	0.05556	0.3101
PrecAnnCold	-0.14092	0.10809
Prec2YRCold	-0.1323	0.16211
Prec3YRCold	-0.13958	0.23365
Prec4YRCold	-0.08936	0.23563
Prec5YRCold	-0.06615	0.2868
Prec6YRCold	-0.08521	0.30288
Prec7YRCold	-0.00916	0.29336
Prec8YRCold	-0.05055	0.30514
Prec10YRCold	-0.20801	0.30931
PrecAnnWarm	0.12288	0.17617
Prec2YRWarm	0.22639	0.24094
Prec3YRWarm	0.15356	0.23577
Prec4YRWarm	0.17757	0.19267
Prec5YRWarm	0.27106	0.26509
Prec6YRWarm	0.26659	0.19922
Prec7YRWarm	0.26418	0.20342
Prec8YRWarm	0.20815	0.13607
Prec10YRWarm	0.23638	0.2648
NAOMonth	-0.32646	-0.0914
NAOAnn	-0.10702	-0.00499
NAO2YR	-0.11335	0.06488
NAO3YR	-0.03347	0.11947
NAO4YR	-0.0579	0.08905
NAO5YR	-0.07568	0.04181
NAO6YR	-0.05314	0.07568
NAO7YR	-0.06578	0.0237
NAO8YR	-0.03722	0.02485
NAO10YR	-0.04915	-0.0124
NAOAnnCold	-0.072	-0.00356
NAO2YRCold	-0.02838	0.02361
NAO3YRCold	-0.09387	0.12591
NAO4YRCold	-0.01775	0.09402
NAO5YRCold	-0.02831	0.11385
NAO6YRCold	0.03193	0.10157

NAO7YRCold	-0.05516	0.04278
NAO8YRCold	-0.02157	0.06376
NAO10YRCold	-0.13928	0.00895
NAOAnnWarm	0.00992	-0.0558
NAO2YRWarm	-0.06825	-0.01966
NAO3YRWarm	-0.01295	-0.03419
NAO4YRWarm	-0.01192	0.00462
NAO5YRWarm	0.0123	0.00657
NAO6YRWarm	-0.01758	0.00138
NAO7YRWarm	-0.05516	0.04278
NAO8YRWarm	0.0046	0.00037
NAO10YRWarm	0.07895	-0.00197
NAMAnn	-0.17685	0.1409
NAM2YR	-0.19272	0.16781
NAM3YR	-0.21421	0.26841
NAM4YR	-0.17059	0.27706
NAM5YR	-0.2168	0.31507
NAM6YR	-0.15823	0.33417
NAM7YR	-0.2672	0.31626
NAM8YR	-0.22745	0.30655
NAM10YR	-0.22193	0.30144
AMOMonth	0.46743	-0.11234
AMOAnn	0.4552	-0.12102
AMO2YR	0.49546	-0.10876
AMO3YR	0.48843	-0.10634
AMO4YR	0.4884	-0.11542
AMO5YR	0.48563	-0.11499
AMO6YR	0.48431	-0.1365
AMO7YR	0.48457	-0.14399
AMO8YR	0.48453	-0.15462
AMO10YR	0.47183	-0.1538
AMOAnnCold	0.51533	-0.0306
AMO2YRCold	0.52612	-0.05841
AMO3YRCold	0.53611	-0.09324
AMO4YRCold	0.54697	-0.0815
AMO5YRCold	0.53162	-0.10716
AMO6YRCold	0.54761	-0.09969
AMO7YRCold	0.53931	-0.11736
AMO8YRCold	0.54993	-0.12245

AMO10YRCold	0.53418	-0.12539
AMOAnnWarm	0.37395	-0.1173
AMO2YRWarm	0.43197	-0.13612
AMO3YRWarm	0.41637	-0.12029
AMO4YRWarm	0.42734	-0.1366
AMO5YRWarm	0.42353	-0.13222
AMO6YRWarm	0.41486	-0.13765
AMO7YRWarm	0.4112	-0.15202
AMO8YRWarm	0.40973	-0.16353
AMO10YRWarm	0.40182	-0.16211
Air	0.33943	-0.23752
LandAg	0.40241	-0.41959
LandRes	-0.38707	0.45284
LandInd	0.33528	-0.49125